# Multiple Scale Theoretical Insights on the Switching Behavior of Chemisorbed Azobenzene

by

Christopher Rodney Leon Chapman
B.Sc., University of Victoria, 2009

A Thesis Submitted in Partial Fulfillment of the
Requirements for the Degree of

MASTER OF SCIENCE

in the Department of Chemistry

Multiple Scale Theoretical Insights on the Switching Behavior of Chemisorbed Azobenzene

by

Christopher Rodney Leon Chapman

B.Sc., University of Victoria, 2009

Supervisory Committee

Dr. Irina Paci, Supervisor

(Department of Chemistry)

Dr. Dennis K. Hore, Departmental Member

(Department of Chemistry)

Dr. David W. Steuerman, Departmental Member

(Department of Chemistry)

**Supervisory Committee**

Dr. Irina Paci, Supervisor
(Department of Chemistry)

Dr. Dennis K. Hore, Departmental Member
(Department of Chemistry)

Dr. David W. Steuerman, Departmental Member
(Department of Chemistry)

## ABSTRACT

Azobenzene derivatives have been shown to act as a molecular switch when exposed to an applied electric field. Many applications require the switching molecule to be adsorbed on a surface. The behavior of chemisorbed *N*-(2-mercaptoethyl)-4-phenylazobenzamide on a Au(111) surface has been investigated using a mean-field theoretical approach for azobenzene in alkylthiol monolayers and density functional theory calculations at the zero-density limit. Azobenzene switching in monolayers was found to be dependent on surface coverage, as well as the strength and polarity of an electric field. In the zero-density regime, azobenzene derivatives adopted parallel and upright geometries for both trans and cis isomers. Charged states for upright, adsorbed structures were also analyzed and were found to lower the isomerization energy barrier.

# Contents

# List of Tables

# List of Figures

# ACKNOWLEDGEMENTS

I would like to thank:

**my parents,** for their love and support.

**Irina Paci** for her guidance, insight, patience and passion for science.

**NSERC,** for financial support.

**The University of Victoria,** for financial support.

# Chapter 1

# Introduction

## 1.1 Azobenzene as a Molecular Switch

A molecular switch is a molecule that can change between two or more stable states as a result of changes in its external environment. Most molecular switches are reversible, but they can also be irreversible, like systems that behave as a fuse. The switching process can be triggered by a variety of factors, such as pH, temperature, electromagnetic radiation, chemical stimuli, electric fields or electronic tunneling. Molecular switches have been known in science for a long time, pH indicators being a classic example. At the opposite end of the spectrum, the complex chains of reactions leading to a true/false type of response, such as the genetic regulation [2,3] and signal transduction pathways [4], are biological examples of molecular switches.

Molecular switches are being examined as components in nanotechnology designs. In order for a molecule to be considered for such designs, there must be a change in a chemical or physical property upon switching. Where the switching behavior leads to a change in molecular geometry, the molecular switch can serve as a molecular motor [5,6].

An archetypal example of a molecular switch in chemistry is the azobenzene molecule. Azobenzene and its derivatives exhibit a well-known cis-trans isomerization of the azo (-N=N-) group that leads to large geometrical changes in the otherwise rigid molecule. The more thermodynamically-stable trans isomer has two coplanar phenyl rings whereas the less stable cis isomer has its phenyl rings twisted away from each other. The cis form is not planar due to steric hindrance between hydrogen atoms on neighboring phenyl rings. Consequently, there is a break in the conjugation along the N=N bond. Coupled to its chromophore character due to an extended $\pi$-system, this geometrical change upon isomerization has led to a broad range of practical applications for azobenzene derivatives. They include classical dye manufacturing and chemical sensors [7-11], optical data storage [12-14], photobiological switches [15,16], polymer additives for photoactive materials [17] and the promotion of alignment changes in liquid crystals [18], to name a few. Similar changes in azobenzene molecules tethered to metal surfaces may lead to applications such as switches in molecular electronics [19-21].

The isomerization process has been well studied, particularly in the excited state, and three channels have been proposed for cis-trans isomerization [22-26]: an inversion channel through bending of a single CNN angle, a rotation channel around the CNNC torsional angle and a concerted inversion channel in which both CNN angles change simultaneously. Figure 1.1 shows the rotation and non-concerted inversion pathways. The reaction pathway depends on the excitation energy and the availability of free volume for rotation, but recent theoretical studies suggest that high barriers make the non-concerted inversion pathway unlikely in the excited state [25,26]. Rotation has been found to be the favored mechanism for photoisomerization [24,26-29]. In this pathway, azobenzene is promoted to the first excited state where the NN bond order becomes one, undergoes rotation of the CNNC dihedral until it reaches the energy

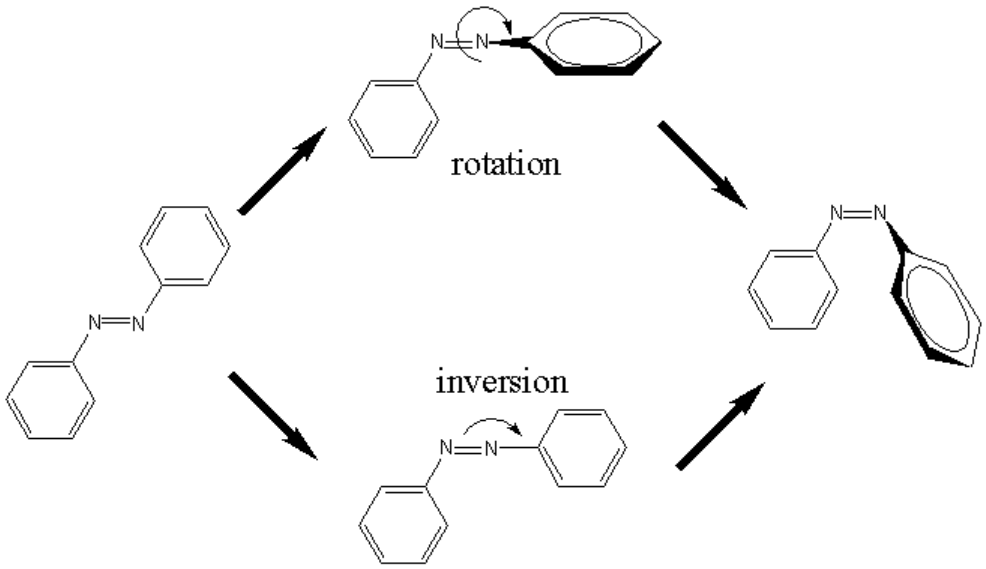


Figure 1.1: Schematic of the inversion and rotation mechanisms of azobenzene trans-cis isomerization.

minimum of the first excited state, relaxes to the ground state and then undergoes further rotation to form the cis isomer [24,26,29].

Ground-state isomerization of many azobenzene derivates has also been studied theoretically [30-34]. Fuschel et al. [35], in particular, discussed the isomerization of neutral and charged surface-bound azobenzene species. In the gas phase, neutral azobenzene molecules were found to have an isomerization energy barrier on the order of 1 eV, the exact value dependent on the substituents attached to the phenyl rings. The non-concerted inversion and rotation pathways were analyzed and the authors found that the inversion and rotation energy barriers were lowered for cationic species. For anionic azobenzene derivatives, only the rotational barrier decreased. The effect of the surface was then included in the form of a work function.

Adsorbed azobenzene derivatives have the ability to switch between two conductance states, that are usually attributed to cis and trans isomers. Scanning tunneling

microscopy (STM) experiments suggest that self-assembled monolayers (SAMs) of adsorbed azobenzene undergo reversible cis-trans isomerization when exposed to light [1,19,36-40]. Photoillumination studies by Levy et al. [39] and Comstock et al. [40] have shown that weakly bound, physisorbed *tert*-butyl azobenzene converts under UV illumination between a low conductance state and a high conductance state in closely packed SAM structures. The low conductance state is generally attributed to the trans isomer, oriented parallel to the substrate, whereas the high conductance state is attributed to the cis isomer, with one benzene ring parallel to the substrate and the other roughly perpendicular to it. The geometry in the adsorbed phase also appears to be significantly affected by substituents in STM studies. Morgenstern et al. [41,42] performed STM studies of 4-amino-4-nitroazobenzene on Au(111) surfaces and observed both trans and cis forms to be parallel to the surface.

In contrast, strongly bound, chemisorbed azobenzene derivatives with alkylthiol linkers form different structures. Experiments on such systems were performed by Kumar et al. [19] and Weidner et al. [1] Current understanding suggests that in these monolayers, the high conductance state is the trans isomer since the extended conjugated system is prevented by surrounding molecules from interacting with the substrate (Figure 1.2). Upon isomerization, the benzene ring located furthest from the surface moves downward, resulting in a state with lower conductance [43].

## 1.2 Density-dependent Switching of Azobenzene Monolayers

For many nanotechnology applications involving molecular switches, the material must be immobilized on a solid surface, rather than present in the liquid or gas

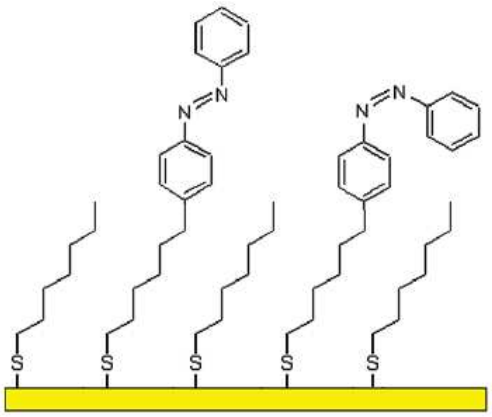


Figure 1.2: Trans and cis isomers of a chemisorbed azobenzene derivative embedded in an alkylthiol matrix. The trans isomer has a larger molecular height than the cis isomer.

phase. The presence of the surface adds significant complexity to the switching process through a number of factors. A fundamental issue is that the molecule can be either chemisorbed or physisorbed on the surface, which influences its behavior with respect to other important factors, such as monolayer density and surface quenching. Another challenge lies in assembling molecules on a surface in an ordered fashion. Further complications arise from the fact that molecular properties in the adsorbed state differ from those in solution or the gas phase.

While the switching behavior of physisorbed azobenzene monolayers is nearly independent of the surface coverage [44], azobenzene switching is strongly dependent on the density of the SAM for chemisorbed structures. At high densities, molecules in chemisorbed azobenzene monolayers are found standing up, nearly perpendicular to the surface. Densely packed monolayers of azobenzene derivatives have generally shown poor photoisomerization yield [37]. This is thought to be because of the different geometry of the cis isomer. The cis azobenzene structure has a significantly larger footprint than the trans form, which leads to inhibition of the cis-trans isomerization

process [1]. At high surface coverage, the available free volume is insufficient to allow isomerization to occur, as shown in Figure 1.3. Exceptions to this were noted when collective isomerization of the monolayer occurred for rigid azobenzene derivatives [36,45]. Solutions to the density problem have been found through use of bulkier groups such as *tert*-butyl for chemisorbed azobenzene [38-40], use of bulky surface binding groups [1] or, in co-adsorption cases, the use of substituent chains that bring the photochromic group on top of the surrounding alkylthiol monolayer [19]. These bulky substituents also serve to distance the azobenzene moiety from the metallic substrate, thus reducing surface quenching of the photoisomerization process.

On the other hand, Elbing et al. [36] showed that in extended, fully conjugated azo systems such as azo-biphenyl moieties, the highly ordered high-density monolayer can exhibit collective switching when illuminated. When these authors used spacers such as methyl substituents on the biphenyl rings, molecules in the lower-density monolayer switched independently, in a fashion similar to that observed for unsubstituted azobenzene.

We found that an alternate interpretation of the density-related suppression of trans-cis isomerization processes is based on lateral interactions. In mixed monolayers, lateral interactions between switching molecules and the matrix play a role in the stabilization of one or both of the conductance states [46]. Needle-like trans-azobenzene molecules can interact, as well as pack, with surrounding molecules more effectively than cis-azobenzene molecules. As the density increases, the lateral interactions become stronger.

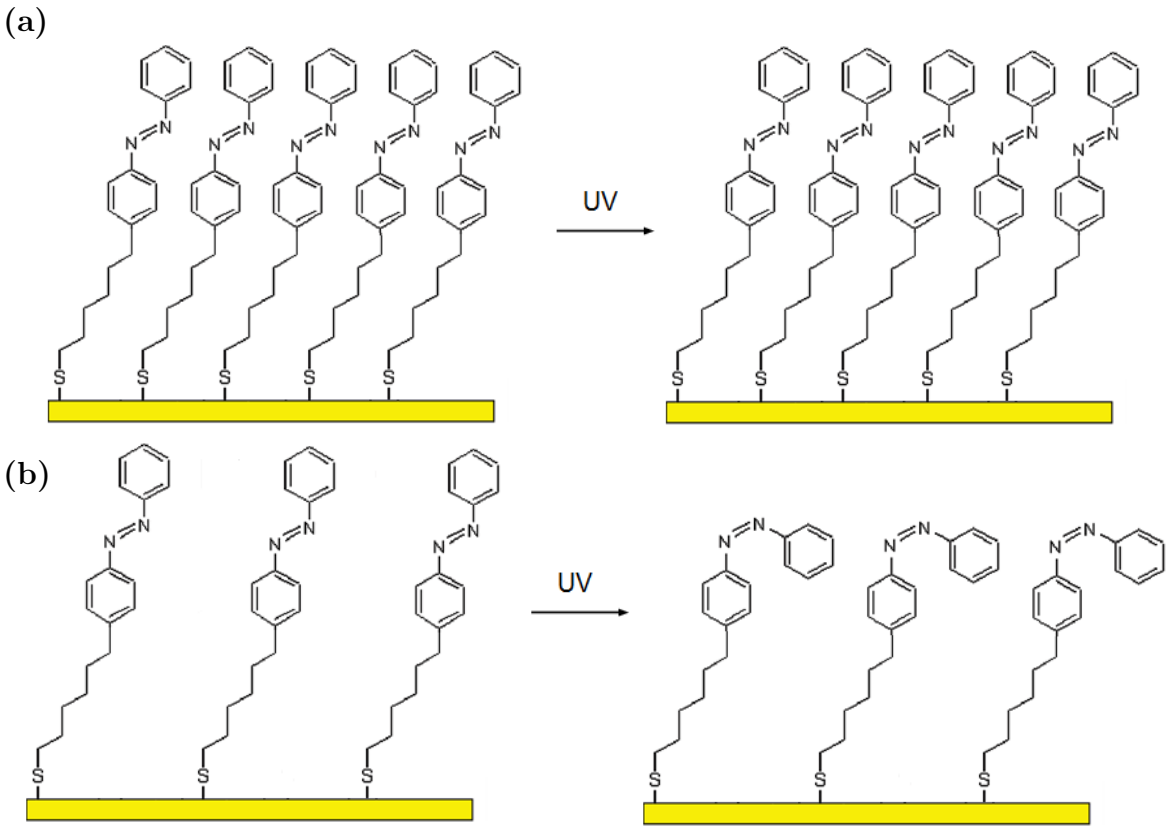


Figure 1.3: Schematic of azobenzene monolayers with densities (a) high enough to inhibit trans-cis isomerization and (b) low enough to allow trans-cis isomerization to occur. Adapted from Reference [1].

## 1.3 Field-induced Switching of Azobenzene

Recent studies have suggested that adsorbed azobenzene can undergo isomerization without photoillumination or electron tunneling: the electric field created by the STM tip is sufficient to overcome the isomerization energy barrier [47-49]. Other systems have also been shown to switch between conductance states when an electric field was applied [50-52]. In these cases, isomerization is thought to occur because of the field-dipole coupling. There is a difference in the permanent dipole moment between the two isomers as a result of variation in the configuration of the phenyl rings and azo group. Consequently, the field-dipole coupling energy can preferentially stabilize one azobenzene isomer over the other.

In cases where binding to the surface occurs through highly flexible alkyl spacers, dipole-field coupling may produce conformational changes in the spacer that lead to changes in the molecular height of the adsorbed molecule [49]. This adds complexity to an already challenging path toward developing an understanding of the switching process in these systems. Moreover, particular care must be taken to discern between different kinds of switching when performing STM studies of optical isomerism (i.e. switching due to field coupling, electron tunneling or UV radiation).

Yasuda et al. [47] observed conductance switching in STM studies of mixed, chemisorbed, alkylthiol/azobenzene monolayers. At boundary and pit sites, molecules exhibited a low current form at low voltage, which underwent fast reversible switching to a high-current form at voltages above 0.25 V/nm. Azobenzene molecules adsorbed within the monolayer did not show any switching capabilities. The authors interpret the motion as a trans-cis isomerization. Das and Abe [49] offer an alternate interpretation of the switching process using density functional theory, arguing that the high isomerization barrier makes the process unlikely at the reported voltages. They

propose that the switching behavior may be due to rotation around one of the single bonds in the linker groups and conclude that orientation of the carbonyl (C=O) group in the linker portion of the molecule, as well as the azo group, are primarily responsible for the field-dependent switching. However, Das and Abe neglect the importance of the surface on the conformation of the chemisorbed azobenzene derivative.

Field-induced switching has also been studied on physisorbed azobenzene monolayers [41,48,53-55]. Alemani et al. [48] demonstrated experimentally that roughly 10% of all physisorbed trans-azobenzene molecules, with tert-butyl groups at the ortho positions, converted to the cis isomer at both positive and negative voltages. By varying the distance between the STM tip and the surface, they found that the isomerization was caused by the electric field rather than tunneling electrons since isomerization was observed even at large tip-surface distances. The authors interpreted that the cis isomer, having one phenyl ring oriented away from the surface, can couple to the electric field more effectively as a result of a higher polarizability along the surface normal in addition to its permanent dipole moment.

## 1.4 Mean Field Theory

Mean field theory is used extensively for many-body systems possessing complex interactions between particles. Determining thermodynamic properties for such systems, by taking into account the interactions explicitly, is challenging even for a simple 2D Ising model [56]. Mean field theory provides a way to simplify the system such that thermodynamic functions can be solved analytically. In a mean field approximation (MFA), all of the specific interactions felt by an individual particle from neighboring particles are assumed to form an average potential [56,57]. In other words, pair interactions are replaced by their average value, thereby reducing an n-body problem

to a single-body one. The approximation is valid for systems that are well-ordered and do not have large fluctuations [58].

For SAMs, the mean field potential is determined largely by the orientation and nature of the molecules, and the overall order of the SAM [59]. Appropriately applied and for relatively small molecules like *N*-(2-mercaptoethyl)-4-phenylazobenzamide and dodecanethiol used in this thesis, a MFA can yield good qualitative agreement with experiment, and, more importantly, is capable of providing significant physical insight.

The MFA was first developed and applied to materials that are capable of forming nematic phases by Cotter and Wacker [59] and Gelbart [60]. Their method was later extended and used in numerous applications, including polymeric thin films [61-63], surface-protein interaction studies [64], and mixed monolayers [65]. This thesis employs the MFA to determine the strength of the attractive and repulsive interactions between the host alkylthiol matrix and azobenzene molecules.

# Chapter 2

# Methodology

## 2.1 Derivation of the Helmholtz Free Energy Expression within the MFA

Understanding the behavior of an equilibrium system with a large number of molecules can be achieved using statistical thermodynamics. Characterizing a large system based on microscopic properties without keeping track of each individual particle is computationally inexpensive and allows for generalization [58]. Perhaps the most important thermodynamic parameter is the total energy, and we have chosen to derive the Helmholtz free energy because our system, described in Section 2.2 and Chapter 3, is modeled at constant temperature and volume. The Helmholtz free energy for a multi-component system with restricted molecular conformations has previously been derived in the MFA for phase separation in SAMs [65] and nematogenic solutions [59,66,67]. The main derivation points for treating field-induced molecular switching are discussed here. In general, the Helmholtz free energy $F$ [56] is given by

$$F = E - TS, \tag{2.1}$$

where $E$ is the internal energy of the system, $T$ is the temperature and $S$ is the entropy of the system. Helmholtz free energy is the thermodynamic function used at constant volume, temperature and number of molecules [56], which makes it suitable for modeling our system.

Information about equilibrium statistics in condensed matter systems can be obtained by locating minima on the typically complex free energy surface for that system. In statistical thermodynamics, the Helmholtz free energy of a system of $N$ particles in a volume $V$ (or area for this study) is directly calculated from the configurational partition function

$$\beta f = -\frac{\rho}{N} \ln Q_N. \tag{2.2}$$

Here, $f$ is the Helmholtz free energy per unit volume, $\rho = N/V$ is the number density and $Q_N$ is the configurational partition function,

$$Q_N = \prod_{\nu=1}^{k} (N_\nu!)^{-1} \int d\Omega^N d\mathbf{r}^N e^{-\beta U(\mathbf{r}^N, \Omega^N)}, \tag{2.3}$$

where $\beta = 1/k_B T$, $k$ is the number of components, $N_\nu$ is the number of molecules of component $\nu$, $U$ is the system's potential energy and $\Omega$ and $\mathbf{r}$ denote the molecular orientations and positions, respectively. The $N_\nu!$ term accounts for indistinguishable particles. The $6N$-dimensional integral of Equation (2.3) can be estimated numerically in approaches such as molecular dynamics and Monte Carlo simulations, or analytically using a series of approximations that allow separation of variables. An analytical solution, which can allow generalization without substantial computational cost, is developed here (below) by following others [59,65] in making valid approximations.

In a most general sense, a $k$-component monolayer is under investigation. Molecules

are adsorbed on a substrate and there is a distribution of molecular orientations. The STM experiment generates an electric field, considered here to be uniform and stationary. The system is physically defined by its potential energy, as is the case in most types of statistical approaches. In this case, the potential energy can be expressed as

$$U = V^{attr} + V^{*} + V^{ads} + V^{field}. \tag{2.4}$$

Here, $V^{attr}$ is given by all the attractive intermolecular interactions and $V^{*}$ is constituted by the overall intermolecular repulsions. $V^{ads}$ and $V^{field}$ are the adsorption energy and the coupling energy between molecular dipoles and the external field of the STM tip, respectively.

Orientation-dependent integrals are handled by considering a number of discrete orientations, $n$, available to each molecule by dividing the unit sphere into solid angles of $\Delta\Omega$:

$$n = \frac{4\pi}{\Delta\Omega}. \tag{2.5}$$

This transforms the integrals over $\Omega$ into nested sums over discrete orientations

$$\int d\Omega^{N} = \left(\frac{\Delta\Omega}{4\pi}\right)^{N} \sum_{N_{1,1}} \cdots \sum_{N_{k,n}} \prod_{\nu=1}^{k} \prod_{\sigma=1}^{n} N_{\nu}!(N_{\nu,\sigma}!)^{-1}, \tag{2.6}$$

where $N_{\nu,\sigma}$ is the number of molecules of type $\nu$ with orientation $\sigma$. Molecules in the system have a specific distribution of orientations that form the largest term in the partition function summation. Using the largest term approximation [57] reduces the configurational partition function to a $3N$-dimensional integral over positions

$$Q_N = \left(\frac{\Delta\Omega}{4\pi}\right)^{N} \prod_{\nu=1}^{k} \prod_{\sigma=1}^{n} (N_{\nu,\sigma}!)^{-1} \int d\mathbf{r}^{N} e^{-\beta(V^{attr}+V^{*}+V^{ads}+V^{field}+V^{iso})}. \tag{2.7}$$

Two-centre integrals coming from pair intermolecular attractions are determined using the MFA: the attractive potential $V^{attr}(\mathbf{r}, N_{1,1}, \ldots, N_{k,n})$ is replaced by the average potential, $\tilde{V}^{attr}(N_{1,1}, \ldots, N_{k,n})$, which is approximated to be independent of molecular positions. This leads to

$$\begin{aligned} V^{attr} &= \tilde{V}^{attr} \\ &= \frac{1}{2V} \sum_{\nu=1}^{k} \sum_{\sigma=1}^{n} \sum_{\nu'=1}^{k} \sum_{\sigma'=1}^{n} N_{\nu,\sigma} N_{\nu',\sigma'} A_{\nu,\nu'}^{\sigma,\sigma'}, \end{aligned} \tag{2.8}$$

in which $V$ is the total area and the attraction parameter $A_{\nu,\nu'}^{\sigma,\sigma'}$ is the average potential of molecule $\nu$ with orientation $\sigma$ felt by molecule $\nu'$ with orientation $\sigma'$. By invoking the MFA, the attractive term is no longer a function of the intermolecular distance and can thus be brought outside of the integral in Equation (2.7).

Integrals involving the repulsive potential are again treated in a mean-field fashion by replacing them with the excluded area terms. These excluded area terms depend on the type of molecules and their orientation but not on the identity and position of the molecules. The excluded area is based on a hard core potential [57]

$$V^*(\mathbf{r}) = \begin{cases} \infty & \text{if molecules overlap} \\ 0 & \text{otherwise.} \end{cases}$$

The repulsive interaction integral then becomes

$$\int d\mathbf{r}^N e^{-\beta V^*(\mathbf{r})} = \left( \frac{V - V_{ex}}{V} \right)^N, \tag{2.9}$$

where the excluded area $V_{ex}$ is given by

$$V_{ex} = \frac{1}{2N} \sum_{\nu=1}^{k} \sum_{\sigma=1}^{n} \sum_{\nu'=1}^{k} \sum_{\sigma'=1}^{n} N_{\nu,\sigma} N_{\nu',\sigma'} b_{\nu,\nu'}^{\sigma,\sigma'}. \tag{2.10}$$

Here $b_{\nu,\nu'}^{\sigma,\sigma'}$ is equal to the area excluded to a molecule of type $\nu$ with orientation $\sigma$ by the presence of neighbouring molecules of type $\nu'$ with orientation $\sigma'$.

The adsorption and field-dipole coupling energies are also approximated to be independent of position

$$V^{ads} = \sum_{\nu=1}^{k} \sum_{\sigma=1}^{n} N_{\nu,\sigma} h_{\nu,\sigma}; \tag{2.11}$$

$$V^{field} = -\sum_{\nu=1}^{k} \sum_{\sigma=1}^{n} N_{\nu,\sigma} E_z (\mu_z^{\nu,\sigma} + \alpha_{z,z}^{\nu,\sigma} E_z), \tag{2.12}$$

where $h_\nu$ is the molecular adsorption energy, $E_z$ is the electric field strength (applied along $z$), $\mu_z$ is the $z$-component of the dipole moment and $\alpha_{z,z}$ is the $z,z$-component of the polarizability tensor. The external electric field is assumed to be aligned only along $z$, the surface normal.

With these approximations, the logarithm of the partition function becomes

$$\begin{aligned} \ln Q_N &= N \ln\left(\frac{\Delta\Omega}{4\pi}\right) - \left(\sum_{\nu=1}^{k} \sum_{\sigma=1}^{n} N_{\nu,\sigma} \ln N_{\nu,\sigma} - N\right) + N \ln\left(\frac{V - V_{ex}}{V}\right) \\ &\quad -\beta \tilde{V}^{attr} - \beta V^{ads} - \beta V^{field} - \beta V^{iso}, \end{aligned} \tag{2.13}$$

and after some mathematical manipulation, the Helmholtz free energy becomes

$$\begin{aligned}\beta f &= -\rho \ln\left(\frac{\Delta\Omega}{4\pi}\right) + \rho\ln\rho + \rho\beta\sum_{\nu=1}^{k}\sum_{\sigma=1}^{n} x_{\nu,\sigma}h_{\nu,\sigma} + \rho\sum_{\nu=1}^{k}\sum_{\sigma=1}^{n} x_{\nu,\sigma}\ln x_{\nu,\sigma} \\ &+\frac{\rho^2\beta}{2}\sum_{\nu=1}^{k}\sum_{\sigma=1}^{n}\sum_{\nu'=1}^{k}\sum_{\sigma'=1}^{n} x_{\nu,\sigma}x_{\nu',\sigma'}A_{\nu,\nu'}^{\sigma,\sigma'} \\ &-\rho\ln\left(1-\frac{\rho}{2}\sum_{\nu=1}^{k}\sum_{\sigma=1}^{n}\sum_{\nu'=1}^{k}\sum_{\sigma'=1}^{n} x_{\nu,\sigma}x_{\nu',\sigma'}b_{\nu,\nu'}^{\sigma,\sigma'}\right) \\ &-\rho\beta\ E_z\sum_{\nu=1}^{k}\sum_{\sigma=1}^{n} x_{\nu,\sigma}(\mu_z^{\nu,\sigma}+\alpha_{z,z}^{\nu,\sigma}E_z) + \rho\beta V^{iso}, \end{aligned} \tag{2.14}$$

where $x_{\nu,\sigma}$ is the mole faction of molecules of type $\nu$ with orientation $\sigma$.

## 2.2 Application to Azobenzene Switching in Monolayers

The system for our statistical mechanical study presented in Chapter 3 is comprised of three components: dodecanethiol, trans- and cis-*N*-(2-mercaptoethyl)4-phenylazobenzamide (denoted $C_{12}$, TAB and CAB, respectively) chemisorbed on an Au(111) substrate. TAB and CAB can interconvert, but the total proportion of azobenzene in the monolayer is constant. To simplify the free energy expression each component was assumed to have a characteristic tilt angle. In other words, each component adopts a uniform orientation. This assumption is consistent with the well-ordered nature of alkanethiol [68-70] and conjugated [71,72] single-layer SAMs, and leads mathematically to the removal of all sums over orientations in Equation (2.14). Furthermore, molecular orientation is assumed to be independent of density. This is not usually the case in experimental investigations, but has a minor impact in the qualitative results in medium to high coverage monolayers. This is confirmed

by the investigation of tilt angles, evaluated by varying the attractive and excluded volume terms (Section 3.7).

The Helmholtz free energy of the system thus becomes

$$\begin{aligned}\beta f &= \rho\ln\rho + \rho(x_1\ln x_1 + x_2\ln x_2 + x_3\ln x_3) + \rho\beta(x_1h_1 + x_2h_2 + x_3h_3) \\ &\quad +\rho^2\beta A - \rho\ln(1-\rho B) - \rho\beta E_z(x_1\mu_{z,1} + x_2\mu_{z,2} + x_3\mu_{z,3}) \\ &\quad -\rho\beta E_z^2(x_1\alpha_{zz,1} + x_2\alpha_{zz,2} + x_3\alpha_{zz,3}) + \rho\beta x_3\Delta H^{iso}, \end{aligned} \tag{2.15}$$

where the indices 1, 2 and 3 refer to $C_{12}$, TAB and CAB, respectively, and $\Delta H^{iso}$ is the free energy of the trans-to-cis isomerization reaction. $A$ and $B$ are the attractive and excluded volume terms, respectively, and are defined as

$$A = \frac{1}{2}(x_1^2A_{11} + x_2^2A_{22} + x_3^2A_{33} + 2x_1x_2A_{12} + 2x_1x_3A_{13} + 2x_2x_3A_{23}) \tag{2.16}$$

and

$$B = \frac{1}{2}(x_1^2b_{11} + x_2^2b_{22} + x_3^2b_{33} + 2x_1x_2b_{12} + 2x_1x_3b_{13} + 2x_2x_3b_{23}). \tag{2.17}$$

In Equations (2.16) and (2.17), the cross terms are symmetric with respect to molecular exchange which leads to the factors of two inside the brackets.

Desorption events are not considered, which means that the mole fraction of $C_{12}$ is constant. Moreover, because the total fraction of AB is unchanged, the mole fraction of CAB can be expressed as a function of the mole fraction of TAB. This means that

$$x_1 + x_2 + x_3 = 1 \tag{2.18}$$

and

$$x_2 + x_3 = x_{AB}, \tag{2.19}$$

where $x_{AB}$ is the total AB mole fraction. As a result, the free energy can be expressed as a function of just one variable.

Stationary states of Equation (2.15) were found by minimizing the Helmholtz free energy with respect to the mole fraction of TAB, using the expression

$$\begin{aligned} \beta\left(\frac{\partial f}{\partial x_2}\right) &= \rho \ln\left(\frac{x_2}{x_3}\right) + \rho\beta(h_2 - h_3) + \rho^2\beta A' + \frac{\rho^2 B'}{1-\rho B} \\ &\quad -\rho\beta E_z(\mu_{z,2} - \mu_{z,3}) - \rho\beta E_z^2(\alpha_{zz,2} - \alpha_{zz,3}) - \rho\beta\Delta H^{iso}, \end{aligned} \tag{2.20}$$

where

$$A' = x_2 A_{22} - x_3 A_{33} + x_1 A_{12} - x_1 A_{13} + (x_3 - x_{2)} A_{23} \tag{2.21}$$

and

$$B' = x_2 b_{22} - x_3 b_{33} + x_1 b_{12} - x_1 b_{13} + (x_3 - x_2) b_{23}. \tag{2.22}$$

The minimization of the Helmholtz free energy was performed numerically using the Numerical Algorithms Group (NAG) subrouting E04BBF [73]. The subroutine, appropriate for unconstrained searches for a minimum within the interval (0,1) of the minimization variable, is based on cubic spline interpolation. The subroutine uses analytical first derivatives in addition to the input function, and requires continuity for both Equations (2.15) and (2.20). There are no discontinuities in the Helmholtz free energy expression in the full range of TAB mole fractions. The case of the mole fraction of TAB ($x_2$) or CAB ($x_3$) going to zero was avoided since the logarithmic terms in Equations (2.15) and (2.20) would be undefined. Numerical minimizations were performed on the SHARCNET high performance computation consortium.

## 2.3 DFT Calculations using SIESTA

Statistical thermodynamics is useful in obtaining a qualitative understanding of the behavior of a collection of molecules at a finite temperature. However, this method is not suitable for modeling single molecules adsorbed on a surface. To properly treat the behavior of an adsorbed molecule in the zero-density limit, density functional theory (DFT) is employed.

### 2.3.1 DFT Overview

DFT is an *ab initio* electronic structure method in which electron density, rather than wavefunctions, is the variable used to solve the Hamiltonian operator. Electron density is proportional to the probability of finding an electron within a particular volume and integrates to the total number of electrons [74]. Hohenberg and Kohn [75] proved that the external potential is determined by the electron density and that the electron density that minimizes the total energy is the exact ground state electron density.

Figure 2.1 outlines the process of a DFT calculation [74]. Electron density is initially formed by a linear combination of atomic orbitals. The effective potential is calculated from the electron density and the Kohn-Sham equation,

$$E[\rho(\mathbf{r})] = T[\rho(\mathbf{r})] + V_{ne}[\rho(\mathbf{r})] + V_{ee}[\rho(\mathbf{r})], \tag{2.23}$$

is solved, where $\rho(\mathbf{r})$ is the electron density and $T$, $V_{ne}$ and $V_{ee}$ are the electron kinetic energy, nuclei-electron interaction energy and electron-electron interaction energy functionals, respectively.

The main advantage of using DFT over other electronic structure methods is that

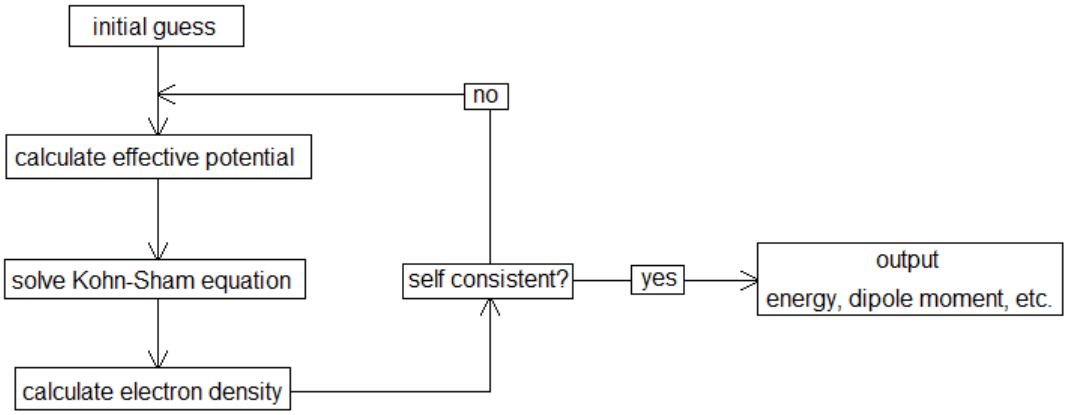


Figure 2.1: Block diagram of a DFT calculation.

calculations, in practice, scale linearly with the number of electrons [74]. Electron density depends only on position, whereas methods employing wave functions depend on position and the number of electrons. As a result, DFT can be used on large systems. However, there are some drawbacks to DFT. The most fundamental problem is that there is no known functional connecting electron density to the kinetic energy or electron-electron interaction energy [74]. Another issue is poor treatment of van der Waals interactions [74]. Improving DFT treatment of dispersive forces is of current research interest [76-78].

### 2.3.2 SIESTA Methodology

The SIESTA [79,80] (Spanish Initiative for Electronic Simulations with Thousands of Atoms) code, version 2.0.2, was used for all DFT calculations, and electron density plots were determined using the DENCHAR utility program. A double-$\zeta$ plus polarization (DZP) basis set was utilized for all atoms in combination with the Perdew-Burke-Erzenhof [81] (PBE) generalized gradient functional and norm-conserving non-

local Troullier-Martins [82] pseudopotentials. For main group atoms, the valence electrons were treated explicitly. For gold, the 5d and 6s electrons were treated explicitly. The use of pseudopotentials contributes significantly to the high efficiency of SIESTA for large systems such as those considered here. The SIESTA code also uses effective core potentials (ECP) for all heavy atoms. Since the behaviour of an adsorbed molecule in the zero-density limit is of particular interest, the unit cells in the calculations were fixed and made large enough such that interactions between neighboring cells is negligible: cubic boxes with 50 Å edges were used which provided sufficient vacuum space.

Despite limitations of traditional DFT methods in describing dispersive interactions, a PBE generalized gradient functional was used. This functional is known to generally underestimate dispersive effects in molecule-surface interactions [83], which is slightly preferable to other nonbonding [83] or overbinding [84] quantum methods applicable to our system size.

For the results presented in Chapter 4 and Section 5.1, the surface was modeled using a two-layer, 128-atom regular Au(111) lattice. In Sections 5.2-5.4, the surface employed was a two-layer, 61-atom regular Au(111) lattice. The surface was minimized for each system using PBE/DZP, with periodic boundary conditions, to remove spurious forces due to mismatch between the ideal (111) lattice and the minimum-energy lattice within the computational method. Surface atoms were then frozen for the remainder of the calculations.

To determine the number of Au(111) layers that are necessary to accurately model molecule-substrate interactions, the surface atomization energies were examined by removing a single gold atom from the top surface layer. The atomization energy is given by

$$E_{atom} = E_N - E_{N-1} - E_1, \tag{2.24}$$

| layers | $E_{atom}$ (eV) |
|---|---|
| 1 | 7.06 |
| 2 | 6.63 |
| 3 | 6.67 |
| 4 | 6.66 |
| 6 | 6.58 |

Table 2.1: Changes in the atomization energy with the number of gold layers. The atomization energy is determined using Equation 2.24.

where $E_N$ is the energy of an $N$-atom surface, $E_{N-1}$ is the energy of the surface with a single atom removed and $E_1$ is the energy of an isolated gold atom. The atomization energy measures the reactivity of a given atom due to an incomplete surface. The atomization energy should be independent of the surface thickness considered, once a sufficient number of layers have been included.

As indicated in Table 2.1, two layers are sufficient to produce a value for $E_{atom}$ that is close to the values obtained using three to six layers. This is consistent with the results of a study by Mavrikakis et al. [85], in which the number of Au(111) layers had no significant effect on the binding energy of carbon monoxide and atomic oxygen for surfaces of more than two layers. Therefore, a two-layer Au(111) surface was used, with a large enough surface area to fully support a chemisorbed AB molecule. A larger surface was utilized in Chapter 4 since all AB conformations were considered. Note that Table 2.1 suggests that more than two layers may be necessary to account for the forces on atoms at or near the surface to be well-converged. However, using more than two layers would be computationally expensive and would have a minimal impact on the accuracy for the systems under consideration here.

# Chapter 3

# Bistability in Mixed Azobenzene-Alkylthiol Monolayers using Mean-field Theory

AB exhibits an interesting response to applied electric fields, as its permanent dipole moment is located along the amide C=O bond while polarizability response occurs along the extended conjugated azobenzene moiety. In an experimental study by Yasuda et al. [47], this azobenzene derivative was observed to undergo conductance switching in low-density defects of the alkylthiol monolayer, but AB molecules within the monolayer did not undergo switching. Although the aim of this chapter is not to explain the results of this particular study, we have chosen to use this system (Figure 3.1) to investigate AB switching at a variety of electric field strengths and densities from a statistical thermodynamic perspective. Section 3.1 outlines the methods of calculating parameters of the Helmholtz free energy expression derived in Section 2.2. An analysis of the impact of the electric field strength, density and other parameters on the ratio between trans- and cis-AB in the monolayer is given in Sections 3.2-3.5.

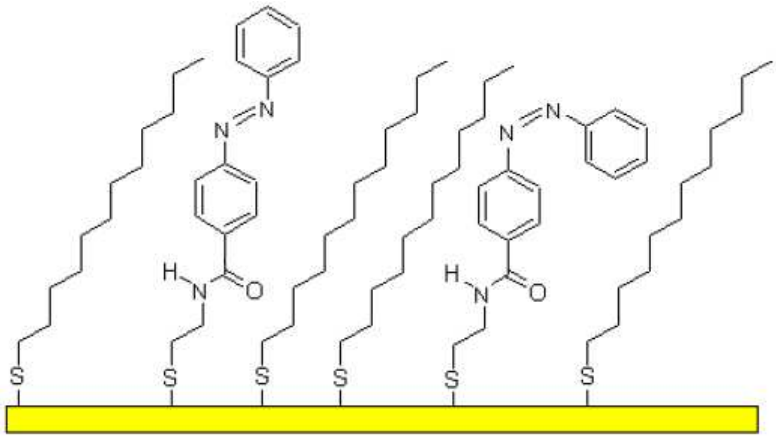

Figure 3.1: Sketch of the mixed $C_{12}$/AB monolayer.

## 3.1 Calculation of Parameters

The attractive interactions ($A$) terms and the excluded volume ($b$) terms were evaluated numerically. The attractive terms included contributions from both van der Waals and permanent dipole-permanent dipole potentials, whereas the excluded volume terms were determined solely from geometrical arguments. Their values are presented in Table 3.1 for three different values of AB tilt angles. In all calculations, it was assumed that the molecules are tilted in the same direction, as shown in Figure 1.2. This assumption is valid since a common tilt direction is a property of SAMs in well-ordered phases [69,70,86,87].

As averages of the attractive interaction potential, $A$ terms were calculated by integrating the pair intermolecular potential over the entire surface where the potential is attractive:

$$A_{\nu\nu'} = \int_{-\infty}^{\infty}\int_{-\infty}^{\infty} u_{\nu\nu'}(x,y)dxdy, \text{ for all values } u_{\nu\nu'}(x,y) < 0. \tag{3.1}$$

| | $A_{\nu,\nu'}$ (kJ·nm$^2$/mol) | | | $b_{\nu,\nu'}$ (nm$^2$) | | |
|---|---|---|---|---|---|---|
| $\nu,\nu'$ | 10° | 20° | 30° | 10° | 20° | 30° |
| 1, 1 | -15.34 | -26.82 | -26.82 | 0.090 | 0.090 | 0.090 |
| 1, 2 | -15.34 | -17.02 | -19.98 | 0.098 | 0.098 | 0.099 |
| 1, 3 | -14.17 | -15.80 | -17.73 | 0.213 | 0.178 | 0.140 |
| 2, 2 | -18.63 | -19.49 | -22.73 | 0.095 | 0.100 | 0.108 |
| 2, 3 | -15.32 | -16.24 | -18.27 | 0.131 | 0.137 | 0.149 |
| 3, 3 | -15.56 | -15.89 | -16.12 | 0.167 | 0.175 | 0.189 |

Table 3.1: Attractive free energy contributions and excluded volume terms for pairs of $C_{12}$, TAB and CAB molecules, calculated for AB tilt angles of 10°, 20° and 30°. In the first column, $\nu$ and $\nu'$ refer to the molecule type, identified as 1 for $C_{12}$, 2 for TAB and 3 for CAB.

The interaction potential $u_{\nu,\nu'}$ is

$$\begin{aligned} u_{\nu\nu'} &= u_{vdw} + u_{dd} \\ &= -\sum_{i=1}^{n}\sum_{j=i}^{m} 4\varepsilon_{ij}\left[\left(\frac{\sigma_{ij}}{r_{ij}}\right)^{12} - \left(\frac{\sigma_{ij}}{r_{ij}}\right)^{6}\right] \\ &\quad + \frac{1}{4\pi\varepsilon_0}\left(\frac{\boldsymbol{\mu}_\nu \cdot \boldsymbol{\mu}_{\nu'}}{r^3_{\nu\nu'}} - \frac{3\left(\boldsymbol{\mu}_\nu \cdot \mathbf{r}_{\nu\nu'}\right)\left(\boldsymbol{\mu}_{\nu'} \cdot \mathbf{r}_{\nu\nu'}\right)}{r^5_{\nu\nu'}}\right). \end{aligned} \tag{3.2}$$

where $\varepsilon_0$ is the vacuum permittivity constant, summation in the Lennard-Jones term is done over the atoms in the molecules $\nu$ and $\nu'$, $\varepsilon_{ij}$ and $\sigma_{ij}$ are the regular Lennard-Jones parameters [88], and $r_{ij}$ is the distance between atoms. Lorentz-Berthelot combination rules [89,90] were used to estimate the mixed Lennard-Jones parameters:

$$\sigma_{ij} = (\sigma_{ii} + \sigma_{jj})/2 \tag{3.3}$$

$$\varepsilon_{ij} = \sqrt{\varepsilon_{ii}\varepsilon_{jj}}. \tag{3.4}$$

In the dipole-dipole interaction terms of Equation (3.2), the intermolecular separation vector $\mathbf{r}_{\nu,\nu'}$ was estimated using the displacement between the amide nitrogen atoms on the azobenzene molecules, because the amide unit is primarily responsible for the

magnitude of the permanent dipole moment.

Polarizability contributions were neglected in the evaluation of the pair potential, for the sake of keeping the attractive interaction terms $A$ independent of the applied electric field. This approximation is equivalent to the neglect of local field effects. There are two considerations that make this a valid approximation. First, the dipole-dipole potential contribution to the $A$ terms was much less than that of the van der Waals potential ($< 2\%$). Second, the dipole-dipole potential is relevant for A terms that involve only AB, and the majority (99%) of the interactions in the monolayer involve $C_{12}$.

The permanent dipole moments and polarizabilities of TAB and CAB were calculated by first optimizing their structures, in the absence of a gold surface, using the Q-Chem [91] electronic structure program, at the B3LYP/6-311G** level of theory. Optimized structures were rotated to a 30°, then single point calculations were performed to obtain permanent dipole moments and polarizabilities. For the remaining tilt angles, the permanent dipole moments and polarizabilities were simply rotated about $z$. The calculated values are presented in Table 3.2. The permanent dipole moment of $C_{12}$ was taken to be zero since alkanethiols have a small dipole moment in comparison to amides. In addition, the polarizability of $C_{12}$ was assumed to be negligible because $C_{12}$ does not contain a $\pi$-system. Furthermore, these terms do not appear in the first derivative of the Helmhholtz free energy.

Excluded volume ($b$) terms were evaluated using a modified Zwanzig model [92]

| $\nu$ | $w$ (Å) | $\ell$ (Å) | $\phi$ (°) | $\mu_x$ (D) | $\mu_y$ (D) | $\mu_z$ (D) | $\alpha_{zz}$ ($10^{-21}$C·nm$^2$/V) |
|---|---|---|---|---|---|---|---|
| 1 | 2.15 | 17.05 | 30 | ≈0 | ≈0 | ≈0 | ≈0 |
| 2 | 2.59 | 16.89 | 10 | -3.34 | -2.22 | 3.44 | 5.48 |
| | | | 20 | -2.69 | | 3.97 | 5.40 |
| | | | 30 | -1.96 | | 4.38 | 5.15 |
| 3 | 4.53 | 12.12 | 10 | -5.30 | 1.93 | 1.67 | 3.51 |
| | | | 20 | -4.93 | | 2.56 | 3.45 |
| | | | 30 | -4.41 | | 3.38 | 3.30 |

Table 3.2: Geometric parameters (width $w$ and height $h$) of Zwanzig prisms used to represent molecules in the monolayer. Dipole moments and polarizabilities along the electric field axis are also included. Molecule type $\nu = 1$, 2 and 3 correspond to $C_{12}$, TAB and CAB, respectively.

for molecules, as illustrated in Figure 3.2 and described by the following equations:

$$
\begin{aligned}
b_{1,1} &= \frac{2dw_1}{\cos\phi_1} \\
b_{1,2} &= b_{2,1} = d\left(w_1\cos\phi_1 + \frac{\ell_1\sin(\phi_1-\phi 2)+w_2}{\cos\phi_2} + w_1\sin\phi_1\tan\phi_2\right) \\
b_{1,3} &= b_{3,1} = d\left(w_1\cos\phi_1 + \frac{\ell_3+w_3\tan\phi_3\sin(\phi_1-\phi 3)+w_2}{\cos\phi_1} + \frac{w_3}{\cos\phi_3} + w_1\sin\phi_1\tan\phi_3\right) \\
b_{2,2} &= \frac{2dw_2}{\cos\phi_2} \\
b_{2,3} &= b_{3,2} = d\left(\frac{w_2}{\cos\phi_2} + \frac{w_3}{\cos\phi_3}\right) \\
b_{3,3} &= \frac{2dw_3}{\cos\phi_3},
\end{aligned}
\tag{3.5}
$$

where the height $\ell$ and width $w$ were measured from the molecular structures, and the depth $d$ was estimated by the distance between hydrogen atoms on a methylene group. Tilt angles were taken from experimental studies of SAMs composed of conjugated molecules [93,94] and alkanethiols [95]. The geometrical parameters used in our calculations for the $C_{12}$, TAB and CAB molecules are presented in Table 3.2, and the calculated values for $b$ terms are included in Table 3.1.

The tilt angle of $C_{12}$ was taken from an X-ray diffraction study of SAMs composed

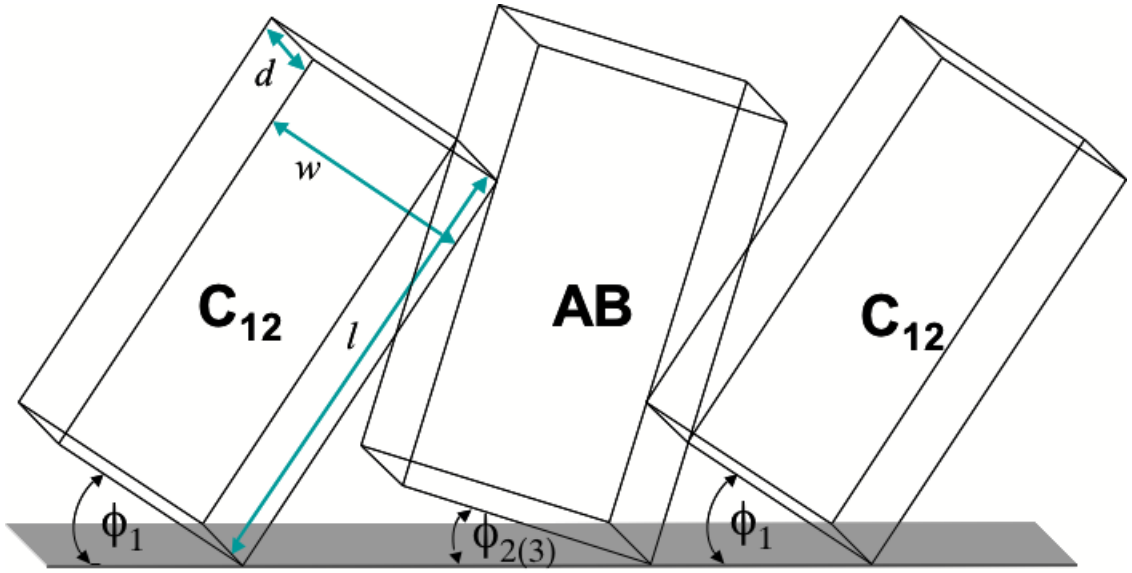


Figure 3.2: Sketch of the geometrical model used to evaluate the excluded volume ($b$) terms. The width $w$, depth $d$, length $l$ and tilt angle $\phi$ for the Zwanzig-type prisms are indicated in the figure. A uniform depth of $d$=1.81Åwas used for all molecules.

of dodecanethiols [96]. There is no specific information in the literature about the tilt angle of azobenzene molecules with short flexible linking groups when embedded in an alkylthiol monolayer. In simulations by Alkis et al. [97], azobenzene inclusions with a single methylene thiol linking group were found to follow roughly the tilt angle of the host alkylthiol monolayer, with an average monolayer tilt, defined from the surface normal, of roughly 30°. Similar angles were reported for pure monolayers of azobenzene bound to the surface through long, flexible linking groups [1]. More rigid, $sp^2$-bound guest molecules bind perpendicular to the surface plane [98]. For biphenyl-based monolayers with alkylthiol linking groups, the dependence of the tilt angle on the length of the alkyl spacer exhibited an odd-even effect [99]: on gold, monolayers with an odd number of methylene groups had a roughly 20° tilt angle, while molecules with even length spacers were tilted at 30°. Most of the calculations

presented in this thesis were performed using a tilt angle of 30° for the AB moiety. The effect of the AB tilt angle is shown in Section 3.7.

The adsorption energy for $C_{12}$ was calculated to be -20.9 kJ/mol from electrochemical data and Au-S and S-H bond strengths [100]. Adsorption energies for both AB isomers are -29.3 kJ/mol [65]. The isomerization energy ($\Delta H^{iso}$) was calculated from the energy difference between the cis and trans isomers using the Q-Chem quantum chemistry package [91], at the B3LYP/6-311G** level of theory, and found to be 24.2 kJ/mol. The entropic contribution was considered to be negligible as there is no change in the number of particles or the phase. A temperature of 298 K was used and the mole fraction of $C_{12}$ was taken to be $x_1 = 0.9$, which is roughly based on coadsorption STM images [47].

## 3.2 Effect of an Electric Field

Two effects are usually examined in discussions of AB switching in STM fields: coupling of the molecular dipole moment with the electric field and the existence of the necessary free volume to accomodate the larger footprint of CAB on the surface. When there is sufficient free volume, switching is understood to occur due to the destabilization of TAB in negative sample biases as a result of coupling between the TAB permanent dipole moment and the STM field [47]. The effect of an applied electric field on the isomerization of AB was investigated by optimizing the Helmholtz free energy at various field strengths. A positive field denotes electrons tunneling from the STM tip to the surface, where the gold surface defines the $xy$ plane and the tip is located on the positive $z$-axis. This is equivalent to a positive sample bias in a STM experiment.

Figure 3.3 shows the percentage of AB molecules that are in the trans form as

a function of field strength. Results for four monolayer densities are shown, when the effect of polarizability was (panel (a)) and was not (panel (b)) included. When the molecular polarizability is neglected (panel b), the system exhibits a monotonous transformation from all-cis at negative fields to all-trans at positive fields. The $z$ component of the TAB permanent dipole is 1.3 times larger than the CAB permanent dipole moment along $z$ (Table 3.2). This leads to a more stabilizing coupling between applied large positive fields and TAB molecules, and the absence of CAB molecules in the monolayer at these fields. At negative fields, both CAB and TAB experience destabilizing contributions to their free energy from permanent dipole-field coupling, but this contribution is again stronger for TAB.

The neglect of polarizability is a poor approximation for these molecules. Azobenzene is highly conjugated, with conjugation extended over both phenyl rings and through the NN double bond. In an electric field, this allows for electron displacement within the molecule. Because of the large polarizability of TAB, unfavorable coupling between the negative field and the permanent dipole of TAB can be overcome at negative fields by induced dipole-field coupling, which is independent of field polarity. This response is stronger in TAB because there is a break in the conjugation at the azo group in CAB.

The resulting curves (Figure 3.3(a)) are characterized by an optimal field strength at which the percentage of CAB in the monolayer is highest. At this field strength, the dipole-field coupling is the most destabilizing for the trans isomer, relative to the cis isomer. At positive fields, as discussed above, the permanent dipole moment of TAB is aligned with the field, which stabilizes the trans isomer and, consequently, inhibits isomerization. On the other hand, when the field is strongly negative, TAB's higher polarizability leads to an induced dipole moment that aligns with the field which is again stronger than that of CAB and leads to TAB dominance.

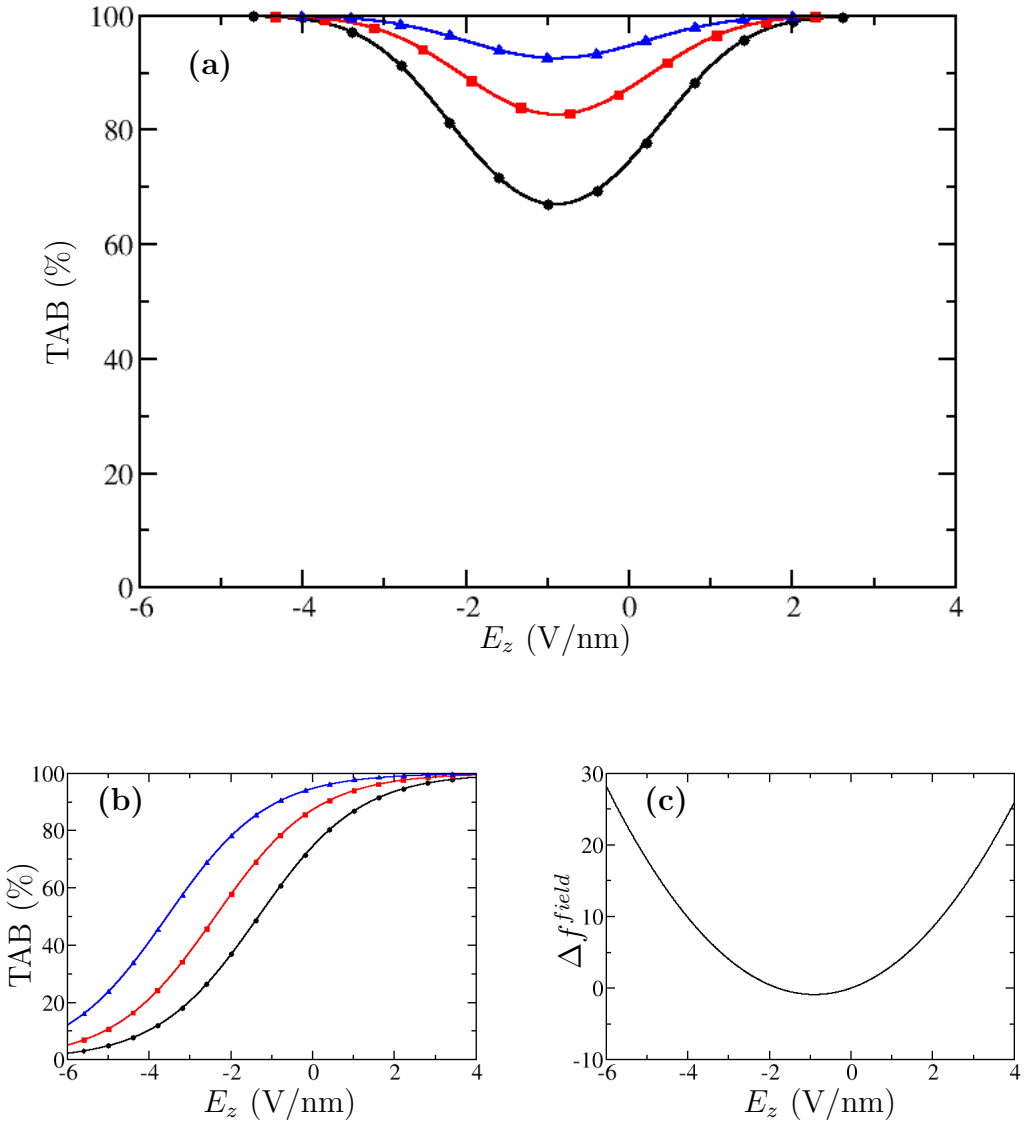


Figure 3.3: Electric field dependence of the fraction of AB molecules in the trans configuration (panel (a)). Black circles, red squares and blue triangles represent densities of 0.1, 1 and 2 molecules/nm$^2$, respectively. Panel (b) is the same except that calculations do not include polarizability. There are 500 data points between each symbol. Panel (c) shows the field dependence on the dipole-field coupling component of the free energy derivative ($\Delta f_{field} = \rho\beta E_z(\mu_{z,2} - \mu_{z,3}) + \rho\beta E_z^2(\alpha_{zz,2} - \alpha_{zz,3})$) in Equation (2.20)

Maximization of CAB in the monolayer occurs at field strengths that minimize the dipole-field coupling terms in the derivative of the Helmholtz free energy (Equation (2.20) and Figure 3.3(c)). Due to the complexity of the mole fraction expression in Equations (2.15) and (2.20) it is difficult to see how this comes about. Interestingly, the field strength at which the monolayer is richest in CAB is independent of the density of the monolayer (Figure 3.3(a)).

## 3.3 Impact of Monolayer Density

Density plays an important role in determining whether field-effect switching can take place. If a monolayer is too compact, switching is seldom observed although collective switching can occur [1]. Collective switching is not possible in the mixed monolayer case analyzed here. As shown in Figure 3.4, calculations also show that TAB-CAB isomerization is inhibited at high densities. There are two factors that can account for this in the formalism. The first factor is attractive interactions in the monolayer. When the density is increased, lateral interactions within the monolayer become more important. TAB interacts more effectively with the surrounding $C_{12}$ molecules (Table 3.1), which means that TAB is favored at high densities. The second factor is that the larger excluded volume of the cis isomer (versus the trans isomer) plays a more important role when the density is high, since there is less room available for isomerization. Note that independent of field strength, the density at which only the trans isomer remains is lower than the typical 5 molecules/nm$^2$ monolayer density for pure alkanethiol systems [101-103].

In order to separate the effects of the attractive and excluded volume factors, they were varied independently and the resulting monolayer composition was determined. Figure 3.5 shows the effect of changing the value of the attractive interaction parame-

ter for the CAB-$C_{12}$ pair. Experimentally, attractive interactions can be modified by using different matrix molecules. Figure 3.5 demonstrates that more attractive CAB-$C_{12}$ interactions result in a decrease in curvature of the density dependence curve, characteristic of an increase in the stability of the cis isomer for higher densities. Less attractive interactions have the opposite effect. Lateral interactions are negligible at zero density so all curves have the same value at that limit.

The excluded volume parameters were also varied by altering the width of the cis isomer. In practice, a relatively wider cis isomer can be achieved by adding bulky substituents to the phenyl rings or a result of a larger CNNC dihedral. Figure 3.6 displays the density dependence of the monolayer composition when the CAB width is doubled and tripled. In contrast to the attractive interactions, altering excluded volume terms had almost no impact on the shape of the density plot. Therefore, there is sufficient free surface area to allow isomerization to occur without a substantial increase in free energy for the densities used in this thesis.

## 3.4 Azobenzene Tilt Angles

The effect of the AB tilt angle on the switching process was estimated by varying AB tilt angles. Specifically, calculations were repeated using tilt angles of 10° and 20°. The $C_{12}$ tilt angle was unchanged since the mole fraction of AB is much smaller than mole fraction of $C_{12}$. Tilt angles impact the different projections of the dipole moment and polarization (Table 3.2), as well as $A$ and $b$ terms (Table 3.1). As the AB tilt angle increases, the AB geometry better matches that of the host alkylthiol, and lateral interactions become more favorable for both TAB and CAB. The dominant $C_{12}$-AB interaction terms are stabilized by 30% for TAB and 25% for CAB when the AB tilt increases from 10° to 30°. At the same time, the excluded volume of CAB

decreases as it packs better in the host monolayer at larger tilt angles. Excluded volume terms for TAB remain essentially unchanged with tilt. Attractive terms are more important in determining isomer stability in the monolayer, as discussed in Section 3.4, and thus it is expected that the TAB isomer is stabilized with increasing tilt angle.

The resulting changes in monolayer composition are presented in Figure 3.7. As expected, the stabilization of TAB is reflected in a shallower minimum for 30° tilt in panel (a) and also in the higher overall percentages of TAB in panel (b). Full conversion of CAB to TAB in the monolayer occurs at lower densities when the tilt angle is larger, again emphasizing the dominance of the lateral interaction effects over excluded volume effects on the switching process.

As the tilt angle is increased, the C=O bond axis progresses toward the surface normal for both isomers. This results in larger values for the $z$ component of the permanent dipole moment and thus more efficient field-permanent dipole coupling. Changes in polarizability with tilt are much less pronounced. This leads to a stabilization of CAB at more positive fields, and thus to a shift to higher voltages for the minimum of the curves in Figure 3.7(a).

## 3.5 Substituent Effects

The effect of the adsorption and isomerization energies on AB switching are presented in Figure 3.8. Like the excluded volume, both of these parameters can be altered by the addition of functional groups. In the standing up structures considered here, the bulk of the surface binding energy is determined by the interaction between gold and the molecular thiol group, which makes the TAB and CAB adsorption energies identical. At lower densities, on the other hand, azobenzene derivatives can lie flat on

the surface in the trans form, and sometimes even in the cis form (see Section 4.1). In these cases, substituents on the benzene rings can also interact with the surface and lead to differences in the adsorption energies of the two isomers.

The field and density dependence of the fraction of AB in the trans form are presented in Figure 3.8(a) and (b), respectively, at different relative adsorption energies. It is apparent from the figures that TAB-CAB isomerization occurs more readily when CAB is more strongly bound to the substrate. From the formalism presented in Section 2.2, this is a direct result of the energetically more stable CAB form that results once it is strongly bound. In practice, however, changes in the strength and type of binding to the substrate have much more complex effects on monolayer behavior. For example, stronger binding by favorable orientation of a substituent can result in a molecule that is less likely to adjust to changes in the monolayer, to lift up from the surface at a given density or to interact as effectively with other molecules in the monolayer.

Finally, Figure 3.8(a) and (b) demonstrate how changes in the isomerization energy affects the proportion of trans molecules as a function of field and density. Not unexpectedly, a more positive isomerization energy (thus a less stable CAB product) leads to more TAB in the mixture. One important note to add is that because of the similar mathematical representation of the adsorption energy and isomerization energy in the Equation (2.15), their effects are also similar. Specifically, a destabilization by 2 kJ/mol of CAB through weaker binding to the substrate leads to an identical simulation to the case in which $\Delta H$ is 2 kJ/mol larger.

## 3.6 Summary

Azobenzene switching in mixed azobenzene-alkylthiol monolayers was investigated using statistical thermodynamics, in which the interaction potential was treated in a mean field fashion. TAB was found to be favored at all electric field strengths, although the amount of CAB was maximized at moderate negative fields. When polarizability was neglected, CAB was dominant at strong negative fields. TAB became more prevalent as the monolayer density increased as a result of attractive, rather than repulsive, lateral interactions. Similarly, increasing the AB tilt angle inhibited switching due to more favorable attractive interactions for the trans isomer at larger tilt angles. Addition of substituents to the phenyl rings can also have an effect on switching through changes in adsorption and isomerization energies.

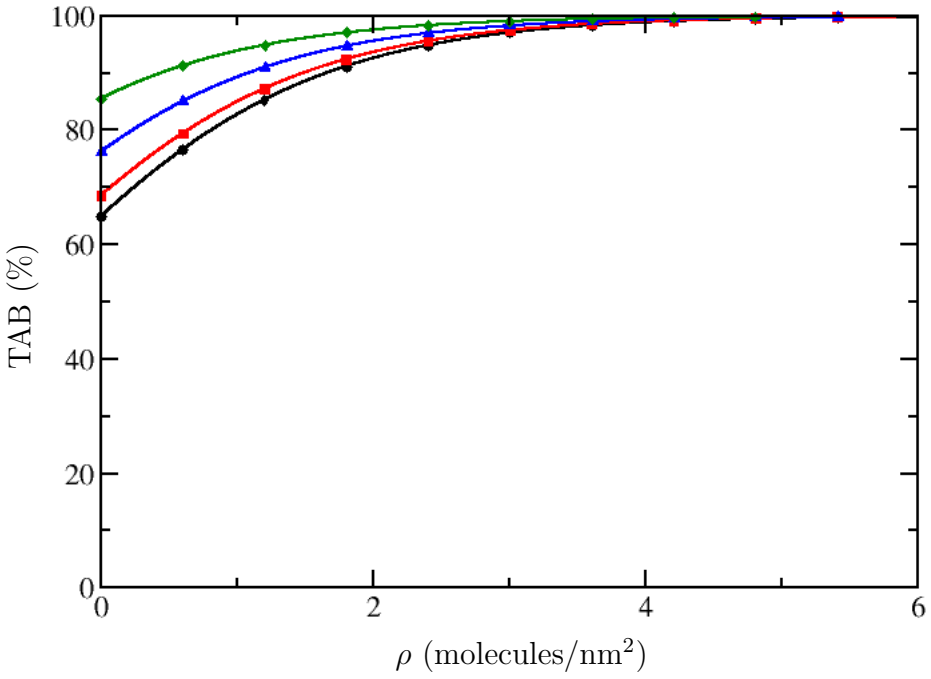


Figure 3.4: Density dependence of the fraction of AB molecules in the trans configuration. Black circles, red squares, blue triangles and green diamonds represent field strengths of -0.9, -1.5, -2 and -2.5 V/nm, respectively. Because the electric field effect is symmetric about -0.9 V/nm (Figure (3.3), the curves for field strengths of -0.9, -0.3, +0.2 and +0.7 V/nm, respectively, overlap the ones shown in the figure. There are 500 data points between each symbol.

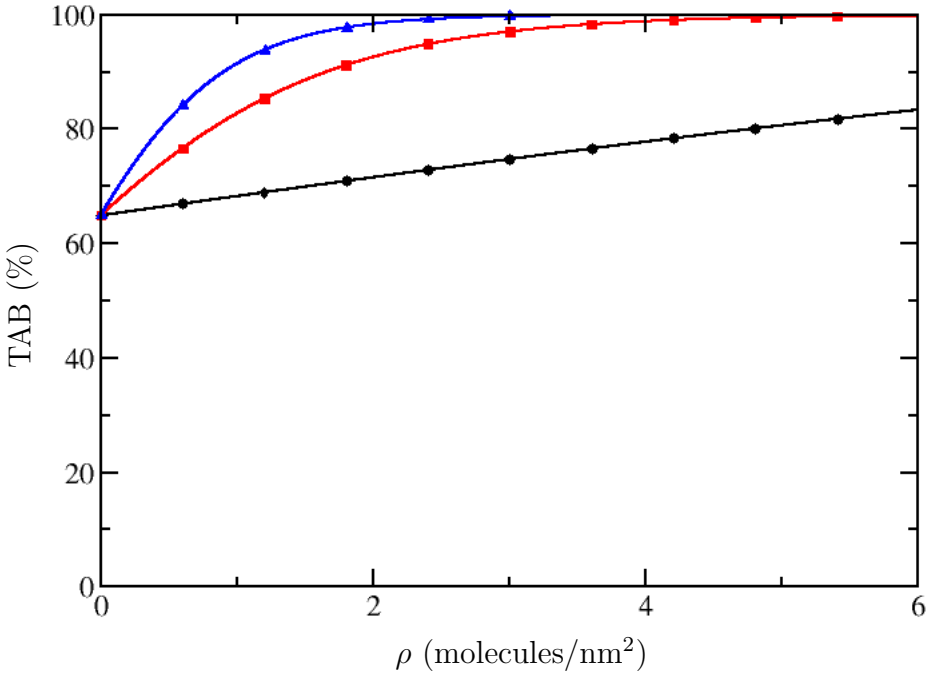


Figure 3.5: The effect of the attractive interactions on the density-dependence of AB switching. From the bottom upward, lines represent increasing values of the $A_{13}$ terms for 30°. Black circles has an $A_{13}$ terms that is 2 kJ·nm$^2$/mol lower than the values given in Table 3.1. Red squares have the same $A_{13}$ value in the table, whereas blue triangles has an $A_{13}$ value that is 2 kJ·nm$^2$/mol higher. There are 500 data points between each symbol.The field was fixed at -0.9 V/nm.

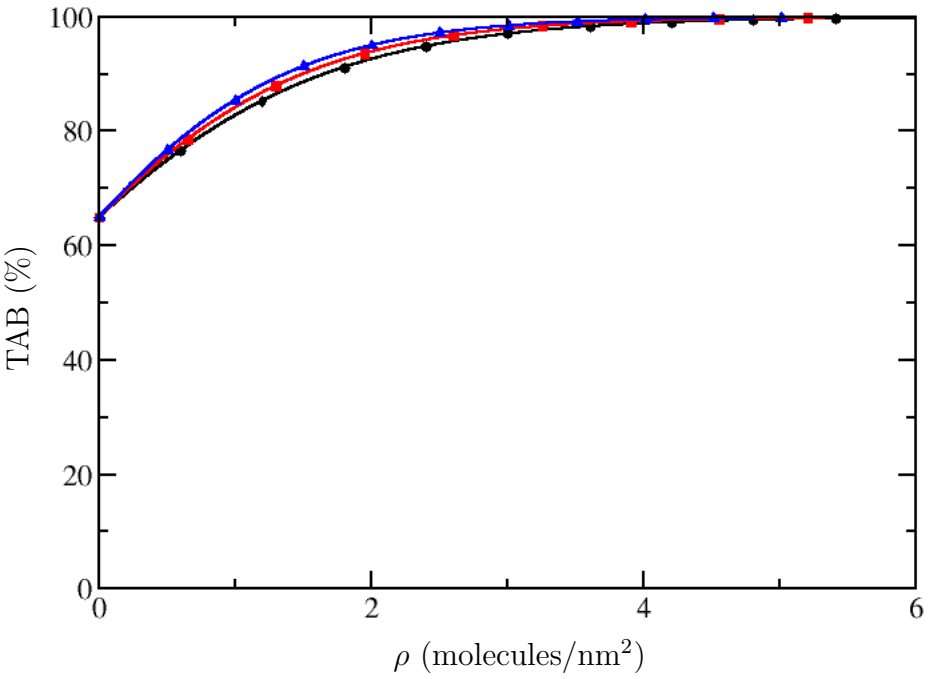


Figure 3.6: Effect of CAB width on the density-dependence of AB switching. Black circles, red squares and blue triangles correspond to widths equal to, double and triple that reported in Table 3.2, respectively. There are 500 data points between each symbol. The field was fixed at -0.9 V/nm.

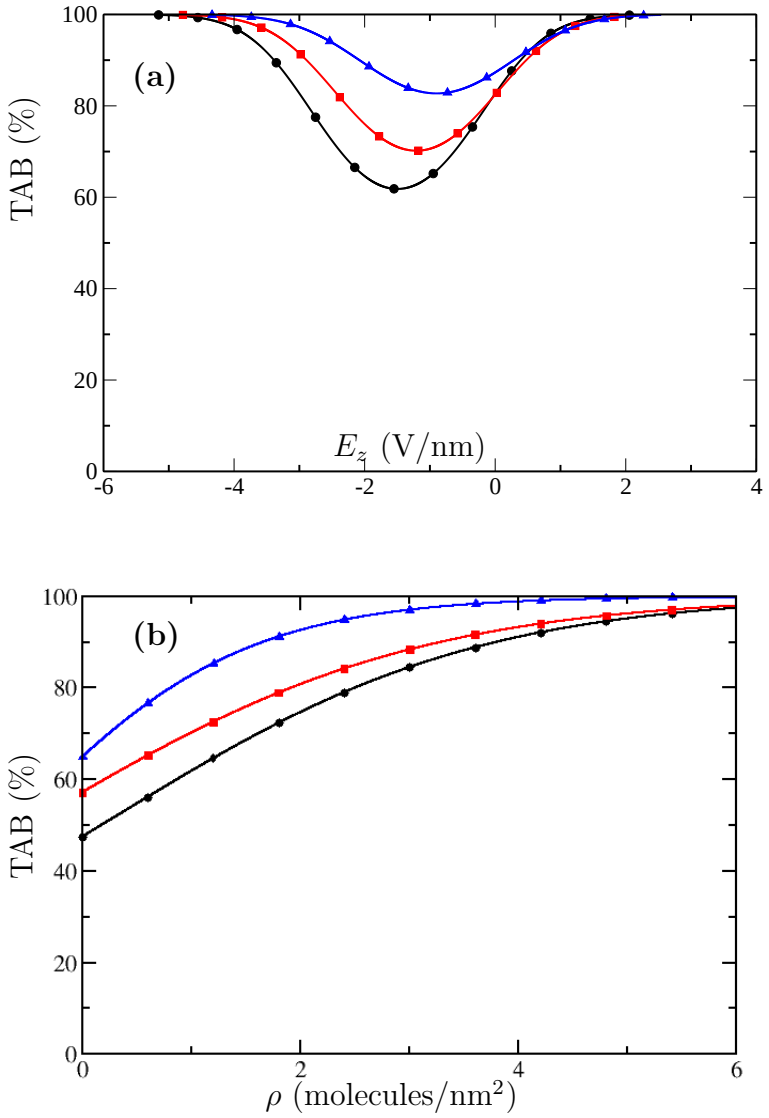


Figure 3.7: Effect of the AB tilt angle on AB switching. Panels (a) and (b) plot the percentage of TAB as a function of applied field and monolayer density, respectively. Black circles, red squares and blue triangles represent AB tilt angles of 10°, 20° and 30°, respectively. There are 500 data points between each symbol. In panel (a), the density was 1 molecule/nm$^2$. In panel (b), the field corresponding to the minimum in panel (a) were used as follows: $E$ = -1.5 V/nm for 10°, $E$ = -1.2 V/nm for 20° and $E$ = -0.9 for 30°.

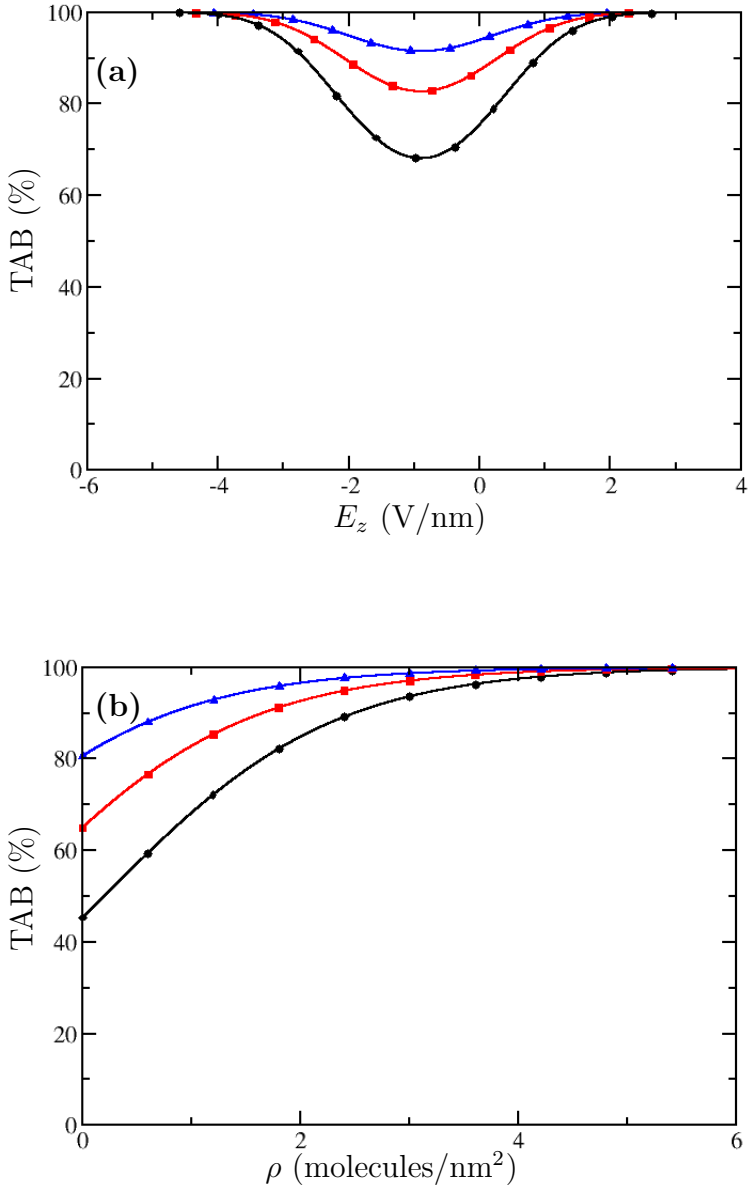


Figure 3.8: Effect of the adsorption and isomerization energies on AB switching. Panels (a) and (b) plot the percentage of AB molecules in trans form as a function of applied field and monolayer density, respectively. Black circles, red squares, and blue triangles represent differences in adsorption energies ($h_2 - h_3$) of 2, 0 and -2 kJ/mol, respectively. Due to the formalism of the Helmholtz free energy, black circles, red squares and blue triangles also represent isomerization energies of 22.2, 24.2 and 26.2 kJ/mol, respectively. There are 500 data points between each symbol. In panel (a), the density was held constant at 1 molecule/nm$^2$. In panel (b), the applied field was -0.9 V/nm.

# Chapter 4

# Conformational Analysis of Chemisorbed Azobenzene Derivatives

We found that in mixed monolayers, switching is fully inhibited at densities significantly lower than those where considerations of molecular footprints are relevant. The behavior of adsorbed molecules at the zero-density limit differ from molecules embedded in a monolayer, since the adsorbed molecule can interact with electrons in the conduction band of the surface. Molecule-substrate interactions may result in different molecular conformations and, consequently, different types of switching. Switching behavior of AB in the zero-density limit has been seen experimentally in surface pit sites [47]. Conformations of AB and an associated butyl derivative in the zero-density limit are explored computationally in Sections 4.1 and 4.2, respectively. AB molecules are, at all times, tethered to the surface through two covalent S-Au bonds. In Section 4.3, inversion and rotation mechanisms are studied for the most stable geometries of trans- and cis-AB.

## 4.1 Equilibrium Structures of $N$-(2-mercaptoethyl)-4-phenylazobenzamide

Structural relaxations were performed with and without an external electric field. The potential energy surface was complicated for the AB and gold system and zero-temperature DFT calculations tended to become trapped in local minima. At least two starting geometries were used for both isomers: one parallel to the surface and the other tilted nearly perpendicular to it. Although parallel structures are lower in energy and thus more stable, optimizations almost never found them when starting from upright initial structures.

The conformational space of AB chemisorbed on a Au(111) surface at the zero-density limit was investigated. Figure 4.1 shows the equilibrium structures of cis and trans AB, found from tilted and parallel starting geometries, and Table 4.1 gives the relative energies and heights of each structure. As is the case with physisorbed azobenzene [40,54,55], the most energetically favorable structure is trans isomer in which the phenyl rings and azo group are oriented parallel to the surface (Figure 4.1(a)). This structure is stabilized by dispersive interactions between the extended $\pi$-system of the AB molecule and the d-electrons of the surface, as well as interactions involving the lone (n) pairs of electrons on the oxygen atom and the surface. The latter interaction causes the conjugation of the amide group to become distorted, and thus the -CO-NH- group is no longer coplanar with the phenyl rings.

In the less-favorable upright trans structure (Figure 4.1(b)), the molecule is oriented approximately 35° from the surface normal. As $\pi$-d interactions are no longer present, strains within the molecule are removed causing the amide group to become coplanar with the azo group and the ethylthiol linker to recover its staggered conformation. However, the substrate interactions do result in the carbonyl group pointing

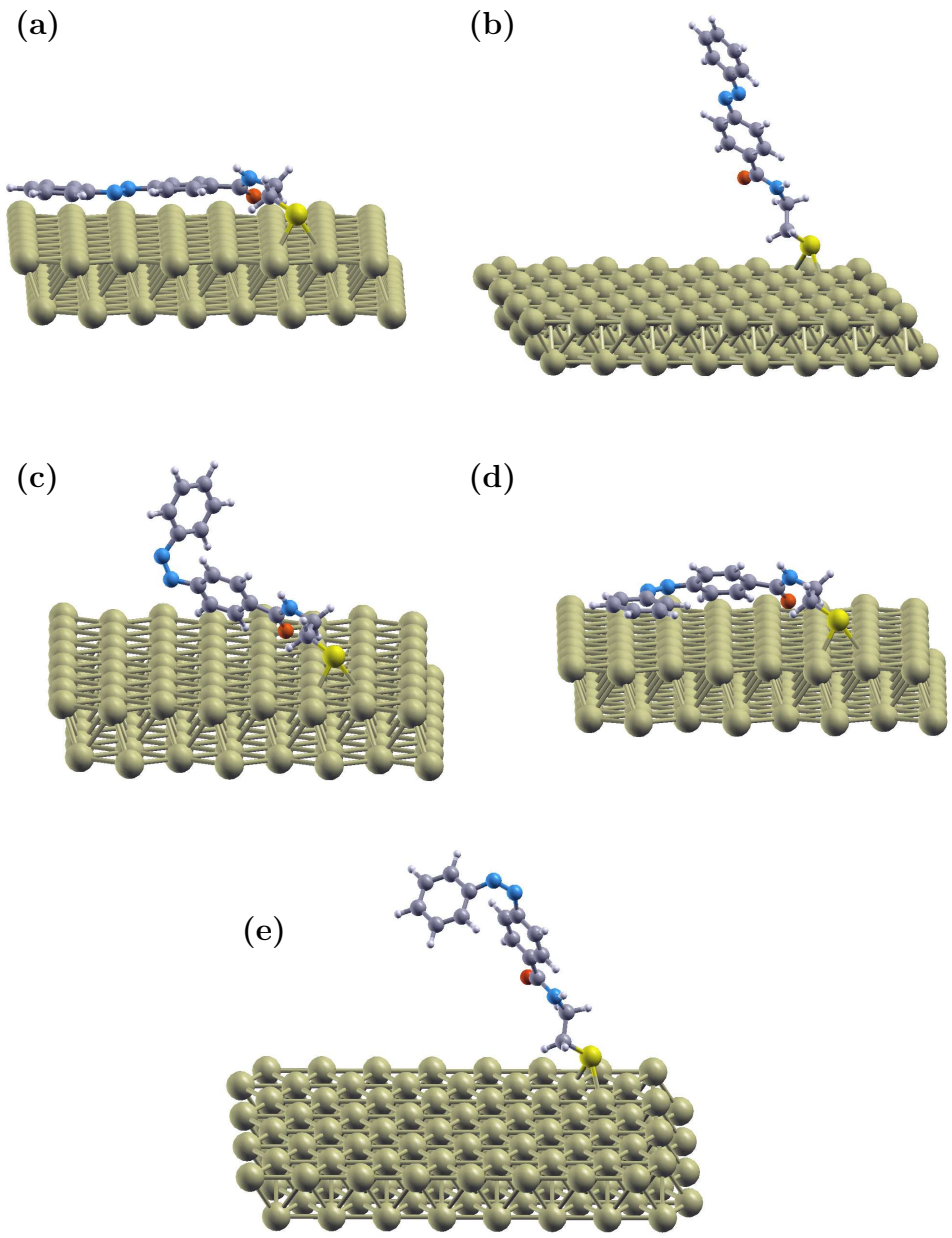


Figure 4.1: Equilibrium structures of trans (parallel (a) and upright (b)) and cis (semiparallel (c), parallel (d) and upright (e)) AB isomers chemisorbed on a Au(111) surface in the absence of an electric field. C, H, O, N and S atoms are grey, white, red, blue and yellow, respectively.

| structure | energy (eV) | height (Å) | desorption energy (eV) |
|---|---|---|---|
| parallel trans | 0.00 | 4.20 | +2.77 |
| upright trans | +2.77 | 15.68 | |
| semiparallel cis | +2.25 | 10.51 | +1.09 |
| parallel cis | +1.11 | 4.64 | +1.14,+2.23 |
| upright cis | +3.34 | 13.05 | |

Table 4.1: Relative energies, heights and desorption energies of AB equilibrium structures.Energies are reported relative to the parallel trans structure.

towards the surface. The desorption energy of 2.77 eV is largely due to the lack of dispersive interactions between the conjugated system and the metal surface in comparison to the parallel structure. The upright trans structure is found predominantly in medium to high coverage monolayers where the lateral dispersive forces and the molecular footprint become important [1,36].

In the gas phase, CAB is non-planar because of steric repulsions between hydrogen atoms in the two phenyl rings. As a result, in principle, only one of the two phenyl rings can be fully parallel to the surface when adsorbed. However, our DFT calculations suggest that the repulsive energy is overcome by $\pi$-d interactions, since most stable cis structure was the one that had both phenyl rings parallel to the surface and the amide group oriented toward the surface (Figure 4.1(c)). The CNNC dihedral angle between the planes of the two rings decreases from 66° in the gas phase to 22° in the parallel cis structure. This type of parallel cis structure has been previously reported by Henzl et al. [54] for physisorbed push-pull azobenzene molecules, but has not been reported in the literature for a chemisorbed azobenzene molecule.

The semiparallel cis structure (Figure 4.1(c)) is more often encountered in STM studies. In this structure, the inner phenyl ring is roughly parallel to the surface while the outer phenyl ring points upwards due to steric repulsion. Also, the semiparallel structure indicates again a competition between coupling to the surface by the phenyl ring and oxygen atom and maintaining conjugation through the amide group. In the

optimized structure, conjugation is maintained and the oxygen-surface coupling is satisfied at the expense of the inner phenyl ring. The oxygen points toward the surface, which leads to a slight tilt of the inner phenyl ring away from the surface parallel. This means that, within the PBE/DZP approximation, $\pi$-d interactions between one phenyl ring and the surface cannot overcome the energy cost of weakening conjugation through the amide group. Tilted initial cis isomers optimize to an upright cis structure (Figure 4.1(e)), which is the least stable structure. This structure has the highest energy due to the lack of dispersive forces between the molecule and the substrate and the inherently less stable cis N=N bond.

When the parallel trans structure is desorbed, it adopts the upright trans structure. However, the desorption of the parallel cis structure is more complicated due to the break in conjugation at the azo group. A partial desorption results in the formation of the semiparallel cis structure and a full desorption results in the formation of the upright cis structure.

Despite deficiencies associated with PBE/DZP-based dispersion and conformation searches at 0 K, this conformational analysis nevertheless gives a good indication of the expected behavior of chemisorbed AB in the zero-coverage limit of STM experiments. In STM experiments, the brightness of an image depends on the molecular height and the local density of states [104]. Molecular heights are therefore expected to correlate well with STM images, as the most visible features are generally phenyl rings. The parallel trans form of AB would be seen as having the lowest height in an STM image. Although the height of the parallel cis structure is comparable to that of the parallel trans structure, the position of the two phenyl rings allows one to distinguish them [54]. The semiparallel cis configuration has one phenyl ring pointing away from the surface, and thus would be seen as two contrasting spots: a darker spot corresponding to the lower phenyl ring and a brighter spot due to the upright

| structure | energy (eV) | height (Å) | $\mu_z^0$ (D) |
|---|---|---|---|
| parallel trans | 0.00 | 5.01 | 1.77 |
| upright trans | +1.71 | 10.15 | 1.39 |
| semiparallel cis | +1.10 | 6.94 | 2.97 |
| parallel cis | +1.21 | 5.22 | 2.00 |

Table 4.2: Relative energies, heights and permanent dipole moments of AAB equilibrium structures in the absence of an electric field. Energies are reported relative to the parallel trans structure of AAB.

phenyl ring. The upright trans and cis structures, which have the largest molecular heights, would be seen as the high, or bright forms.

## 4.2 Equilibrium Structures of 4-Mercaptobutyl-4-phenylazobenzene

The behavior of the derivative 4-mercaptobutyl-4-phenylazobenzene (AAB, alkyl azobenzene) was studied to determine contribution of the n-d coupling terms to the binding energy in the equilibrium structures of AB. Possible effects of the replacement of the amide unit with an ethyl unit are higher flexibility of the linking group and loss of oxygen-surface interactions.

Minima on the zero-field potential energy surface of AAB are similar to those found for the amide derivative (Figure 4.2). Like AB, the most stable configuration of AB the parallel trans structure (Figure 4.2(a) and Table 4.2), which having its entire conjugated system oriented parallel to the substrate. The molecule lies higher above the surface than AB, because of the smaller attraction between the linker group and the surface. Upright trans and semiparallel and parallel cis structures were also found, as shown in Figures 4.2(b)-(d), respectively.

However, their structures show notable differences when compared to the corre-

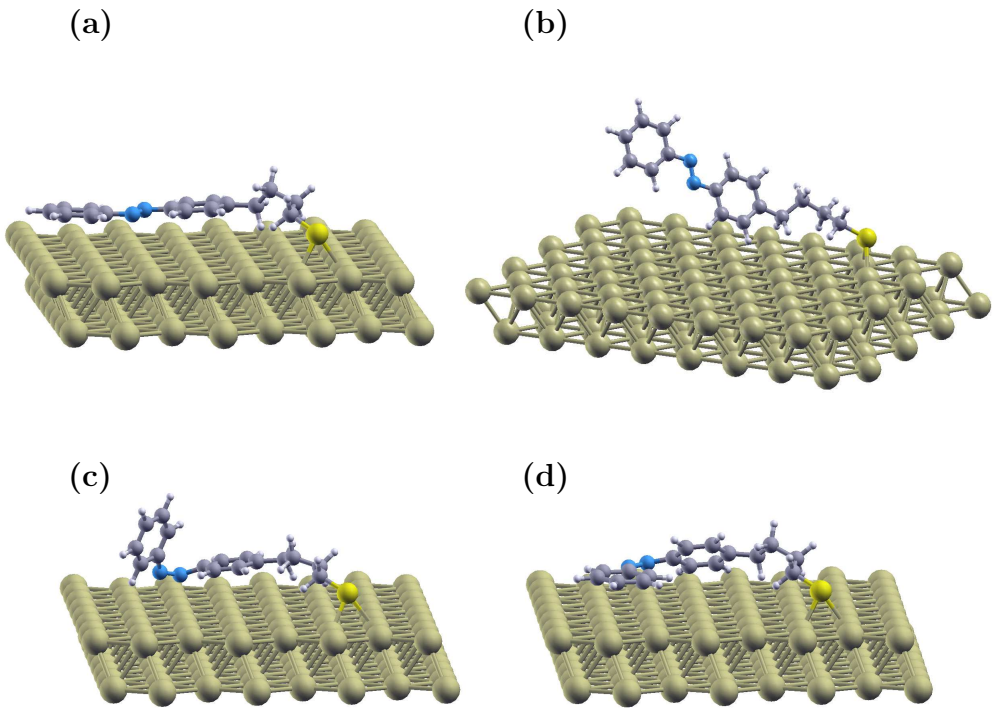


Figure 4.2: Equilibrium structures of trans (parallel (a) and upright (b)) and cis (semiparallel (c) and parallel (d)) alkyl azobenzene isomers chemisorbed on a Au(111) surface in the absence of an electric field. C, H and S atoms are grey, white and yellow, respectively.

sponding amide derivatives. The upright trans structure is significantly closer to the surface, with a tilt angle of approximately 65° from the surface normal. Also, the desorption energy is smaller by 1.06 eV in comparison to the amide derivative because of weaker dispersive interactions between the linker group and the gold surface for AAB. The cis isomer does not follow the same trend as AB. The semiparallel structure is more energetically favorable than the parallel configuration (Table 4.2). This is in part due to steric repulsion in the azo group region of the parallel cis structure. However, the main difference is that the inner phenyl ring of the semiparallel structure can be fully parallel in AAB, because it lacks the intramolecular strains discussed above.

The 1.7 eV desorption energy of trans-AAB is in agreement with experimental data for small aromatic systems such as benzene, which has a desorption energy of about 0.65 eV [105,106]. McNellis et al. [107] find an experimental desorption energy of 1.7 eV for tetra-tert-butyl azobenzene. This agreement may be due to cancellations of errors [108] arising from the inability of PBE to account correctly for dispersion interactions, basis set superposition errors for the small atomic-orbital basis set used here [106,109], and the use of periodic boundary conditions. Note that the desorption energy values are significantly higher than those reported in Reference [105] for plane-wave DFT calculations on unsubstituted, physisorbed azobenzene using the PBE functional.

The equilibrium structures of AAB demonstrate that the carbonyl group of azobenzene influences the adsorbed geometry and its associated energy. Coupling of the oxygen atom to the surface results in either the distortion of the inner phenyl ring from parallel or a loss in conjugation with the neighboring ring. When the amide unit is replaced with an ethyl group, the added flexibility and decrease in surface coupling allows the molecule to adopt lower-energy metastable structures.

## 4.3 Ground State Isomerization Pathways of Parallel Structures

Inversion and rotation pathways for the trans-cis isomerization of AB in the presence of a gold surface was investigated for parallel structures. There are effects of the Au(111) surface that may make these pathways different from the well-studied gas-phase channels: the surface may also stabilize transition state geometries, such as a parallel structure, that would otherwise be thermodynamically unfavorable in the gas phase. Furthermore, the surface restricts the adsorbed AB molecule from adopting certain conformations.

The relaxed inversion and rotation pathways of the parallel trans to parallel cis isomerization in the zero-density limit were performed as follows. Calculations for the inversion channel were done by optimizing the AB structure, except for the CNN bond angle. Rotation channel geometries were optimized in a similar fashion, with the CNNC dihedral frozen instead. The parallel trans structure was the initial configuration for CNN bond angles of 120-175° and CNNC dihedrals of 105-180°. For the remainder of the inversion and rotation calculations, the cis configuration was the starting structure.

Energy profiles for the inversion and rotation pathways are presented in Figure 4.3 and transition state structures are given in Figure 4.4. The inversion mechanism involves a succession of intermediate geometries that have both phenyl rings roughly parallel to the substrate. The azobenzene moiety was planar between the trans isomer and the transition state. As the CNN bond angle was increased further, the inner ring twisted away from the horizontal as a result of steric repulsion between hydrogen atoms on neighboring phenyl rings. The activation energy was found to be 2.31 eV for the trans-to-cis pathway and 0.60 eV for cis-to-trans. The NNC angle (azo group

nitrogen atoms and closest carbon atom of the inner ring) did not change toward a concerted pathway: it changed from 113° near the trans starting point to 137° at the cis structure.

Rotation channels for gas phase isomerization generally have higher activation energies than inversion channels in the ground state but lower barriers in excited states [29,34]. Calculated rotational barriers range in height from 1.6 to 2.4 eV in the ground state, while inversion pathways have barriers of 1.6-2.2 eV [23,26,29,34]. When an adsorbed, parallel AB molecule undergoes isomerization through a rotation mechanism, there is a loss of planarity at the transition state. The energy profile for this mechanism is illustrated in Figure 4.3(b). The ground state energy barrier is approximately 0.45 eV lower than that for the inversion pathway. The transition state closely resembles that of the semiparallel cis structure (see the lower path in Figure 4.4 and Figure 4.1(c)). However, here the inner phenyl ring and azo group is oriented nearly parallel to the surface.

It is important to emphasize that all of the inversion and rotation calculations were performed in the electronic ground states. During the isomerization of AB, the N=N bond is partially broken in both the inversion and rotation mechanisms. Calculations allowed for spin polarization, so they should be able to account for this. However, the mechanisms described here do not apply to light-induced isomerizations, which occur in excited states, or to tunneling-induced transformations that involve charged states along the isomerization pathways. The latter will be discussed in Section 5.4.

## 4.4 Summary

Zero-field conformers of amide and butyl azobenzene derivatives were examined with DFT calculations. The amide derivative was found to have five conformers: parallel

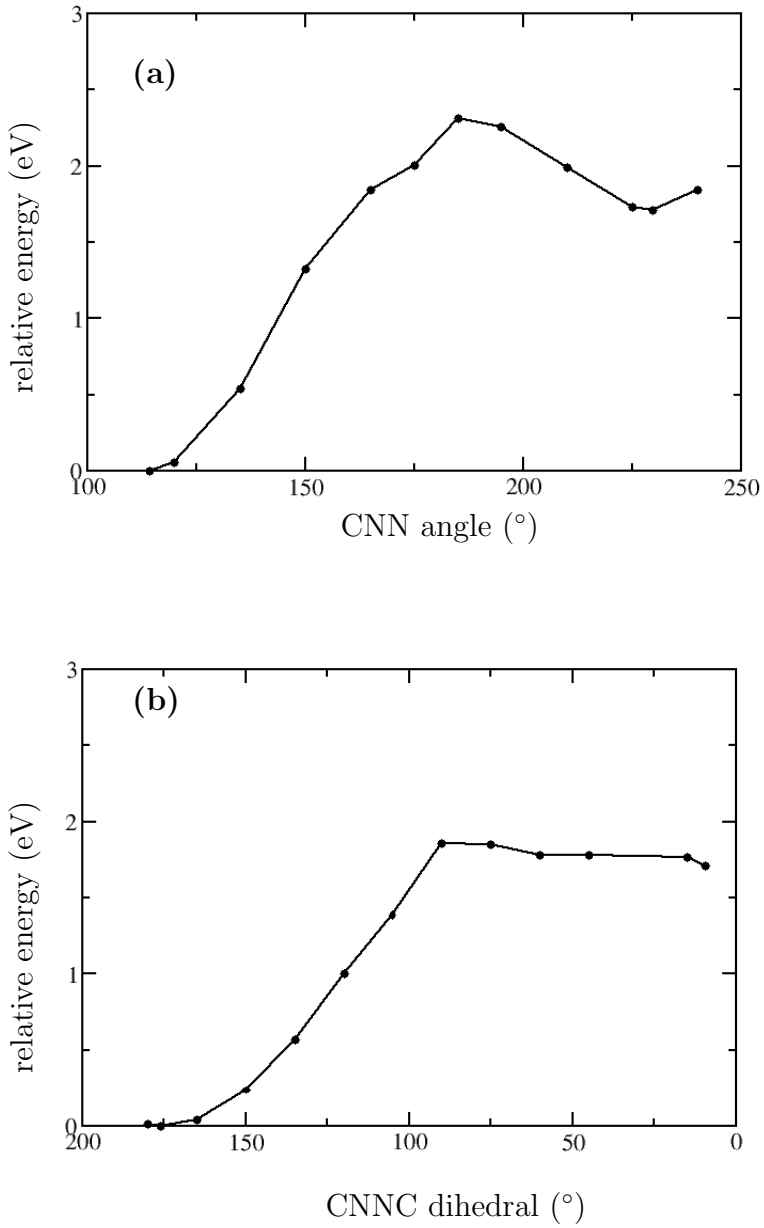


Figure 4.3: Energy profile of trans-cis isomerization of the (a) inversion and (b) rotation pathway for the electronic ground state. In both graphs, the left side corresponds to the trans configuration while the right side corresponds to the cis isomer. Lines are included only for clarity

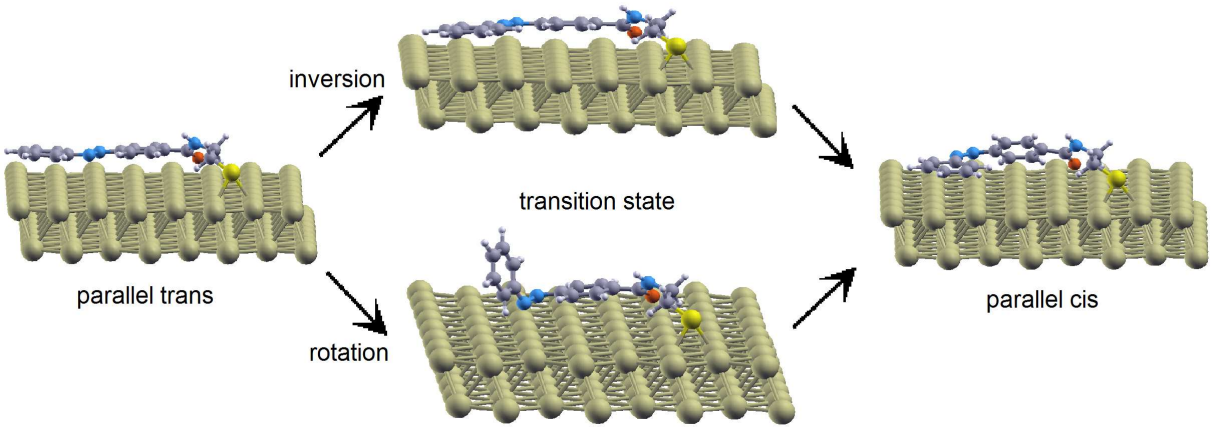


Figure 4.4: Inversion and rotation pathways of azobenzene trans-cis isomerization on a Au(111) surface. C, H, O, N and S atoms are grey, white, red, blue and yellow, respectively.

and upright trans geometries and parallel, semiparallel and upright cis geometries. Parallel structures were the most thermodynamically-stable structures for each isomer. When the ethylamide unit was replaced by a butyl linking group, desorption energies decreased and the semiparallel cis structure became the lowest energy cis geometry. Inversion and rotation channels were also investigated for parallel AB in the electronic ground state. The rotational energy barrier was determined to be 0.45 eV lower than the inversion barrier.

# Chapter 5

# Chemisorbed Azobenzene in an STM Environment

In the previous chapter, parallel structures at zero-density were examined. We found that the energies involved in parallel-based switching are too high. Furthermore, desorption of the parallel geometry to an upright geometry required nearly 3 eV. Scenarios in which upright structures are stabilized over parallel structures include AB buried within single- and multi-component monolayers, as well as in monolayer boundary sites. Also, upright structures interact with an STM tip more effectively due to a larger molecular height, resulting in greater field-dipole coupling and possible short-lived ionic states due to electron tunnelling. In Section 5.1, permanent dipole moments and polarizabilities of AB conformers are calculated and electric field effects are analyzed. Sections 5.2-5.4 discuss AB isomerization and its mechanisms for neutral and ionic states, in both the gas phase and adsorbed phase.

## 5.1 Single Azobenzene Molecules in an Electric Field

### 5.1.1 Dipole Moment Calculations

The electric field of an STM can be responsible for inducing molecular switching, even in cases where electron tunnelling is negligible [48]. When a molecule is exposed to an electric field, there is an interaction between the permanent dipole moment and the field. This interaction may either stabilize or destabilize the adsorbed molecule, depending on the orientation of the permanent dipole moment relative to the electric field. Also, application of a field can result in geometrical changes, as this coupling acts as a torque on the molecule. A free molecule will move to maximize the field-total dipole coupling, whereas adsorbed molecules may have to overcome significant binding energies for motion to occur. Furthermore, coupling between the field and the induced dipole moment can become important when stronger fields are considered, especially for polarizable molecules like AB. For an STM experiment, the electric field is applied along the surface normal, denoted $z$. Therefore, the permanent dipole moment along $z$ and the $z,z$-component of the polarizability tensor are particularly important. The permanent dipole moment $\mu_z^0$ and the $z,z$-polarizability $\alpha_{zz}$ for trans and cis AB conformers described in Section 4.1 are given in Table 5.1. Figure 5.1 describes how $\alpha_{zz}$ was calculated.

**Parallel Structures.** If one is interested only in the dipole moment of the molecule, as is the case for modeling field-dipole coupling of adsorbed molecules, then the molecule needs to be terminated with a functional group. AB was chosen to be terminated with a polar thiol group as well as a non-polar S=S linkage. Dipole moments of the system, which includes both the surface and AB, were also calculated.

| structure | $\mu^0_{z,S-Au}$ (D) | $\mu^0_{z,S-H}$ (D) | $\mu^0_{z,S=S}$ (D) | $\alpha_{z,z}$ (D·nm/V) |
|---|---|---|---|---|
| parallel trans | 2.76 | 1.44 | 2.57 | 0.75 |
| upright trans | 1.20 | 1.70 | 2.87 | 2.94 |
| parallel cis | 2.75 | 1.78 | 2.97 | 0.92 |
| semiparallel cis | 4.10 | 3.41 | 4.60 | 1.63 |
| upright cis | -0.86 | -0.30 | 0.86 | 2.02 |

Table 5.1: Permanent dipole moments at zero field $\mu^0_z$ and calculated $z,z$polarizabilities $\alpha_{zz}$ for the stable structures of cis and trans AB.

For parallel and semiparallel structures, dispersive interactions influence the permanent dipole moment since the relative magnitude differs between adsorbed species and corresponding terminated species (Table 5.1). The orientation of the amide group and relative positions of the phenyl rings have the largest effect on $\mu^0_z$. Since parallel trans and cis configurations have similar amide and phenyl ring orientations, their $\mu^0_z$ values are also similar (Table 5.1 and Figures 4.1(a) and (d)). The semiparallel cis structure has the largest $\mu^0_z$ value because its outer phenyl ring is aligned with the surface normal and its C=O bond axis is closest to this normal (Table 5.1 and Figure 4.1(c)).

**Upright Structures.** Upright trans and cis structures lack dispersive interactions, making the dipole calculation method of little importance. This is evident in Table 5.1, where the relative magnitude of $\mu^0_z$ between isomers does not depend on the terminating group. The value of the dipole moment for surface-bound AB in an upright configuration ($\mu^0_{z,S-Au}$) is more negative than the dipole moment of a thiol-terminated AB molecule ($\mu^0_{z,S-H}$), and even more than the S=S terminated molecule ($\mu^0_{z,S=S}$), due to the inclusion of two highly-polarized Au-S bridge bonds (Table 5.1). The upright cis isomer has a more negative permanent dipole moment in comparison to the upright trans isomer due to the orientation of the outer phenyl ring (ring furthest away from the amide unit), which points towards the surface in the cis configuration (Table 5.1 and Figures 4.1(b) and (e)).

Figure 5.1 shows how the dipole moment changes with an electric field and the

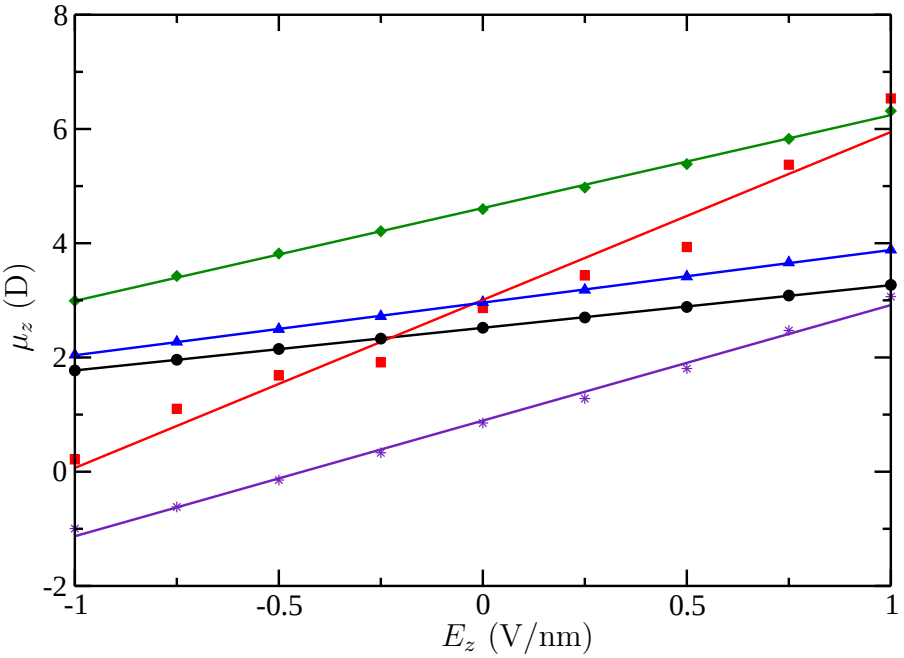


Figure 5.1: Effect of the electric field on $\mu_z$ on five AB geometries. Black circles and red squares represent parallel and upright trans configurations, respectively, and blue triangles, green diamonds and purple stars represent parallel, semiparallel and upright cis configurations, respectively.

slope of each curve corresponds to $\alpha_{zz}$. $\alpha_{zz}$ was determined by a linear regression of the curves in Figure 5.1 and is given for each structure in Table 5.1. Because the structure was allowed to optimize for each field strength, there is a small geometric component of $\alpha_{zz}$, and thus we chose a large range of electric field strengths to determine $\alpha_{zz}$. The quality of the fits shown in Figure 5.1 suggests that this geometric contribution was negligible except for upright trans and cis geometries.

Total dipole moments reported by SIESTA for adsorbed species include a large contribution from the redistribution of charge density within the gold slab when an electric field is applied. To properly account for this contribution, molecular dipole moments in Figure 5.1 were calculated in two steps. First, AB was optimized on a Au(111) surface in an electric field. Then, a single point calculation was performed on

the optimized structure with the surface removed. In this calculation, the Au-S bridge bonds were replaced by a S=S bond, aligned with the $z$ axis. This approximation was used because the S=S group does not contribute significantly to $\mu_z$ and the valency of the sulfur atom is maintained. Note that the interaction between the surface and AB is not accounted for in the determination of $\alpha_{az}$.

Generally, $\alpha_{zz}$ values are larger for structures that have a large conjugated structure aligned or nearly aligned with the $z$-axis. This is the reason $\alpha_{zz}$ is largest for the upright structures, while the parallel configurations have the lowest values. The semiparallel cis configuration had an intermediate value of $\alpha_{zz}$ since one phenyl ring is oriented towards the surface normal and the other ring and amide unit are oriented parallel to the surface (Figure 4.1(c)).

### 5.1.2 Field Effects

The effect of applied fields on the energies of structures is shown in Figure 5.2(a). At each field strength, the structure was optimized in the field and then the energy was calculated. The total energy does, however, include contributions from field-surface coupling. Although the surface has a large polarizability, the contribution of the field-surface coupling to the total energy is the same for each structure. Therefore, field-surface coupling does not affect the energy difference between AB structures.

**Parallel Structures.** The parallel trans structure is energetically favored at all field strengths, even though this structure has the lowest $\alpha_{zz}$ value (Figure 5.2(a)). The energy gap between the various configurations, though, is lowered at high positive and negative fields due to increasing values of $\alpha_{zz}$ for the parallel and semiparallel cis geometries (Table 5.1). There was also little variation in the overall geometry of parallel and semiparallel structures with the electric field: only minor twisting of the

phenyl rings and very small changes in the distance between the oxygen atom and the surface were observed, but the height remained essentially unchanged.

**Upright Structures.** The upright trans structure is stabilized at high field strengths due to a more favorable field-induced dipole coupling. However, this energy is not sufficient to compensate for a lack of stacking interactions in this structure. When a field of 5 V/nm was considered, the upright trans configuration is more stable by approximately 0.5 eV than the parallel structure. However, it is unclear whether the molecules would be chemically stable in experiments which use such high fields. For the entire range of electric field strengths reported, the upright trans isomer was more stable than the upright cis isomer, although the energy difference was lowered at moderate negative fields (Figure 5.2(a)). Unlike parallel structures, both isomers in the upright configuration showed field-dependent geometries. Figure 5.2(b) demonstrates that both isomers adopted a more upright structure. The tilt angle decreased at large field strengths (both positive and negative) for the trans and cis upright structures, but the phenyl rings and amide unit conformation did not change. Only the ethyl linker group underwent minor conformational changes. A more upright structure improves the favorable coupling between the induced dipole moment and the field and, consequently, results in a lower energy structure.

The results presented here suggest that the application of an external electric field does not induce a significant change in the equilibrium structure through field alignment, in the density regimes where lateral interactions are negligible. Thus, these calculations suggest that field-dipole coupling cannot overcome the binding energy in parallel trans-AB to induce the physical desorption necessary for configurational switching.

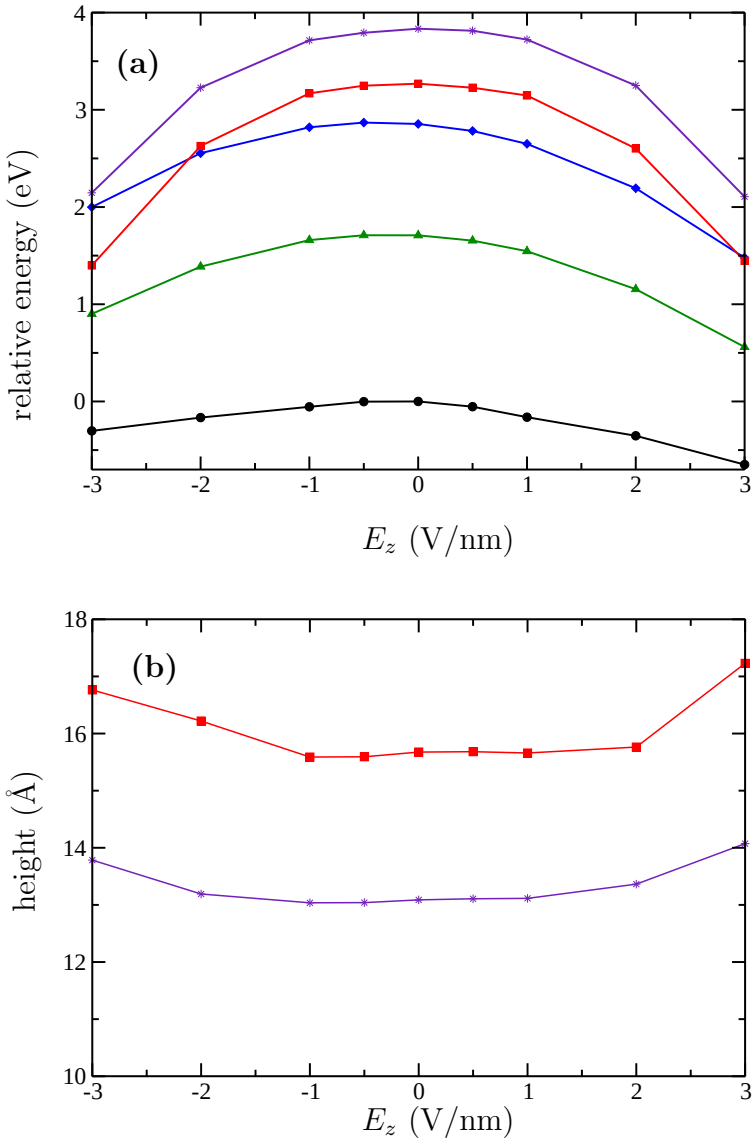


Figure 5.2: Effect of the electric field on (a) the combined energy of AB and the gold surface and (b) the molecular height of upright AB geometries. In panel (a), black circles and red squares represent parallel and upright trans configurations, respectively, and green diamonds, blue triangles and purple stars represent parallel, semiparallel and upright cis configurations, respectively. In panel (b), red squares and purple stars represent upright trans and cis configurations, respectively. Lines are included only for clarity.

## 5.2 Modeling Chemisorbed Ionic States

Cationic and anionic species of both adsorbed and gas phase AB were investigated. The switching process may be due to electron tunneling between the STM tip and the adsorbed AB molecule, in which an ionic intermediate is formed. The charged isomerization pathway can lead to lower activation energies, thus facilitating switching. In an STM experiment, a cationic (anionic) intermediate can be formed when a negative (positive) bias voltage is applied.

Modeling an ionic AB molecule chemisorbed on a gold surface provides a computational challenge. Experimentally, in the case of forming a cation, an electron tunnels from AB to the STM tip since the separation distance between the tip and the surface is too large for electron tunneling from the surface to occur. However, the weakest bound electron for our system is in the highest occupied molecular orbital (HOMO), which is located within the conduction band of the gold surface. Consequently, in removing an electron from the system the positive charge will not be localized on the adsorbed molecule. Rather, an optimization of the electronic structure results in the positive charge being located in the surface. To correct for this effect, an electric field of +1 V/nm along the surface normal was applied, which resulted in part of the HOMO being localized on the adsorbed AB molecule, without significantly altering the molecular conformation. When applying a field, an electron is promoted to a molecular orbital that resides on the molecule and can thus be pulled out by the STM tip. For comparison, a +1 V/nm electric field was also added for neutral, adsorbed AB.

Similarly, determining the behavior of adsorbed AB in the anionic state involves applying an electric field along the surface normal. Applying an electric field of -1 V/nm results in the adsorbed AB molecule being electron deficient and, consequently,

AB is better able to accept an electron into the lowest unoccupied molecular orbital (LUMO). Applying an electric field to an adsorbed AB molecule not only localizes part of the HOMO or LUMO on the molecule itself, but also simulates experimental STM conditions. It should be noted though that without applying an electric field, or if a larger gold surface is used, there is no component of the HOMO or LUMO located near the azo group.

## 5.3 Molecular Orbital Diagrams

**Gas Phase.** A comparison of the geometric parameters and energies for both gas phase and adsorbed AB are given in Table 5.2. For gas phase optimizations, the geometry around the azo group changes for both isomers in going from a neutral to a charged species. For the trans isomer, the only notable change is a decrease in the N=N bond length for the cation and an increase in the bond length for the anion. This is attributed to an electron being removed from the HOMO of the neutral molecule in the case of forming a cation, and adding an electron to the LUMO in the case of forming an anion. The trans AB HOMO (Figure 5.3(a)) is overall non-bonding, although there is a small amount of antibonding character in the N=N region. The trans AB LUMO (Figure 5.3(c)), on the other hand, is largely antibonding, especially in the azo region. Therefore, adding an electron to the LUMO weakens the N=N bond and, as a result, the bond lengthens.

In comparison to the trans isomer, ionic states of the cis isomer in the gas phase exhibited larger geometrical differences around the azo group. In addition to changes in the N=N bond length, there were large changes in the CNNC dihedral angle in going from an uncharged species to an ionic one. This is mainly due to electron repulsion between the nitrogen lone pairs. The HOMO of cis AB (Figure 5.3(b)) shows C-N

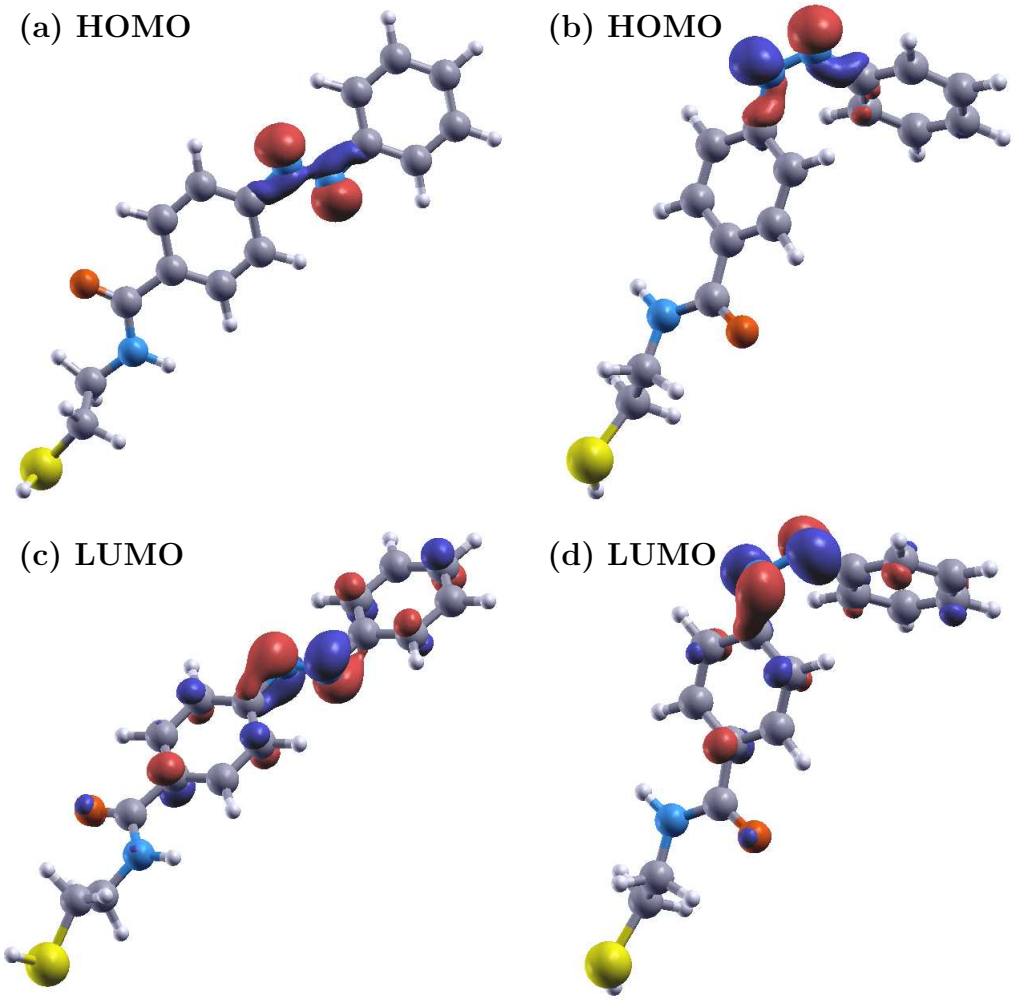


Figure 5.3: PBE/DZP frontier orbital diagrams for gas phase trans (panels (a) and (c)) and cis (panels (b) and (d)) AB. C, H, N, O and S atoms are grey, white, blue, red and yellow, respectively.

| isomer | state | $r_{NN}$ (Å) | CNN (°) | CNNC (°) | $\Delta E$ (eV) |
|---|---|---|---|---|---|
| gas phase | | | | | |
| trans | neutral | 1.28 | 113.5 | 177.0 | |
| | cation | 1.24 | 113.8 | 167.6 | |
| | anion | 1.33 | 112.2 | 176.6 | |
| cis | neutral | 1.23 | 237.4 | 12.6 | 0.51 |
| | cation | 1.24 | 229.8 | 30.5 | 0.38 |
| | anion | 1.32 | 238.2 | 39.7 | 0.58 |
| adsorbed phase (upright) | | | | | |
| trans | neutral | 1.28 | 113.8 | 178.0 | |
| | cation | 1.27 | 116.5 | 177.1 | |
| | anion | 1.29 | 112.7 | 117.5 | |
| cis | neutral | 1.26 | 237.3 | 14.3 | 0.62 |
| | cation | 1.25 | 235.2 | 15.3 | 0.59 |
| | anion | 1.27 | 237.6 | 16.3 | 0.60 |

Table 5.2: N=N bond lengths ($r_{NN}$), CNN bond angles and CNNC dihedrals of trans and cis AB in the gas phase and adsorbed to a gold surface, and trans→cis isomerization energies ($\Delta E = E_{cis} - E_{trans}$). The geometries for neutral and cationic adsorbed AB were determined in the presence of a +1 V/nm electric field normal to the surface. The anionic adsorbed AB geometries were determined in the presence of a -1 V/nm electric field normal to the surface.

bonding and N=N antibonding, whereas the lobes of the LUMO (Figure 5.3(d)) are primarily localized on the nitrogen atoms and are antibonding in character. The CNNC dihedral increases such that the lobes on the nitrogen atoms do not overlap as effectively and, consequently, the lone pair repulsion is lowered. Both the HOMO and LUMO show good qualitative agreement with those calculated by Fuchsel et al. [35]

**Adsorbed Phase.** For adsorbed AB, however, conformational changes are not nearly as pronounced relative to gas phase (Table 5.2), since a significant portion of the pseudo-HOMO (p-HOMO) and pseudo-LUMO (p-LUMO) is found within the gold surface (Figure 5.4). The ionic orbitals are denoted as p-HOMO and p-LUMO because the orbitals were determined in the presence of an electric field. The orientations of the orbitals localized on AB do match those of the gas phase, indicating

that the application of an electric field did not influence the shape or relative energies of the AB-based orbitals. When a larger surface was used, or when an electric field was not applied, the HOMO and LUMO were found to be only located in the surface. Note that to more accurately model an anionic system, diffuse basis sets should be employed. However, calculations involving diffuse basis sets are computationally expensive, especially for late transition metal elements such as gold, are not straightforward to incorporate in the SIESTA package, and their compatibility with the SIESTA pseudopotentials is debatable. As such, anionic results are presented only for completeness.

## 5.4 Isomerization Pathways of Upright Azobenzene for Neutral and Ionic Species

Out of the three possible AB isomerization mechanisms, only the ground state non-concerted inversion and rotation channels are considered here (see Figure 1.1). Inversion and rotation calculations were carried out as described in Section 4.3, except upright trans and cis geometries were used as initial configurations.

**Gas Phase.** In the gas phase, the inversion and rotation pathways have comparable activation energies for the neutral state, as shown in Table 5.3. This suggests isomerization could proceed through either mechanism in the ground state provided that enough energy is supplied. When AB is cationic, the activation energy for each isomerization mechanism is lowered dramatically (0.84 eV and 0.94 eV for the inversion and rotation channel, respectively), but the rotation path is more favorable than the inversion path when AB is anionic. These results are in good agreement with other azobenzene derivatives studied by Fuchsel et al. [35] in which anionic systems

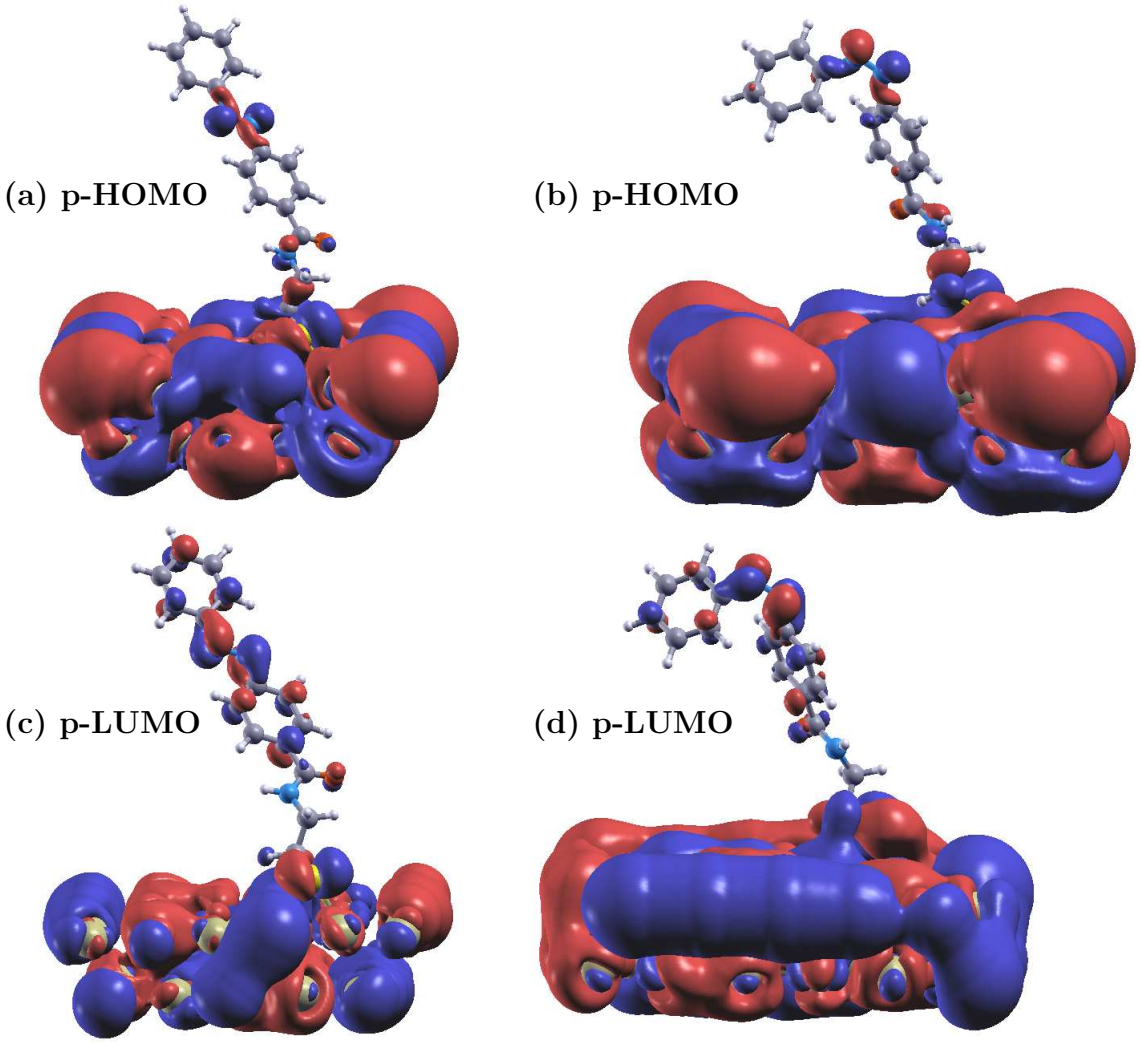


Figure 5.4: PBE/DZP frontier orbital diagrams for adsorbed trans (panels (a) and (c)) and cis (panels (b) and (d)) AB. The p-HOMO and p-LUMO plots were determined in the presence of a +1 V/nm and -1 V/nm electric field, respectively, normal to the surface. The p-HOMO was determined in the cationic state and the p-LUMO was determined in the anionic state. C, H, N, O and S atoms are grey, white, blue, red and yellow, respectively.

| channel | $\Delta E^{\ddagger}_{neutral}$ | $\Delta E^{\ddagger}_{cation}$ | $\Delta E^{\ddagger}_{anion}$ | $\Delta E^{\ddagger}_{neutral}$ | $\Delta E^{\ddagger}_{cation}$ | $\Delta E^{\ddagger}_{anion}$ |
|---|---|---|---|---|---|---|
| | gas phase | | | adsorbed phase (upright) | | |
| inversion | 1.51 | 0.67 | 1.37 | 1.45 | 1.18 | 1.41 |
| rotation | 1.56 | 0.62 | 0.72 | 1.47 | 1.03 | 0.96 |

Table 5.3: Energy barriers for the inversion and rotation channels of the gas phase and adsorbed AB structures. The neutral and cationic adsorbed AB energy barriers were determined in the presence of a +1 V/nm electric field normal to the surface. The anionic adsorbed AB energy barriers were determined in the presence of a -1 V/nm electric field normal to the surface. All values are in eV.

were treated with diffuse basis sets.

Frontier orbitals of the gas phase transition state structures are shown in Figure 5.5. The corresponding orbitals of the adsorbed state were not shown since the majority of the orbital is located on the gold surface (Figure 5.4) and the portion of the orbital localized on the molecule are nearly identical to those in Figure 5.5. Both the inversion and rotation transition state HOMO's (Figure 5.5(a) and (b)) show C-N bonding and antibonding between the nitrogen lone pairs. The trans HOMO (Figure 5.3a), on the other hand, is primarily non-bonding. Therefore, removing an electron from the HOMO will preferentially stabilize the transition state of each isomerization channel, thereby lowering the activation energy.

However, there is a subtle difference between the two transtion state LUMOs. The LUMO of the inversion transition state has stronger double bond character along the C-N than the LUMO of the rotation transition state. This is confirmed by a shorter C-N bond distance for the inversion transition state when AB is negatively charged. Due to the shape of the LUMO around the C-N bond, the inversion transition state has greater antibonding contribution in the azo region than the rotation transition state. Therefore, adding an electron to the LUMO destabilizes the inversion transition state relative to the rotation transition state. This causes the rotation pathway to be favored due to a lower energy barrier.

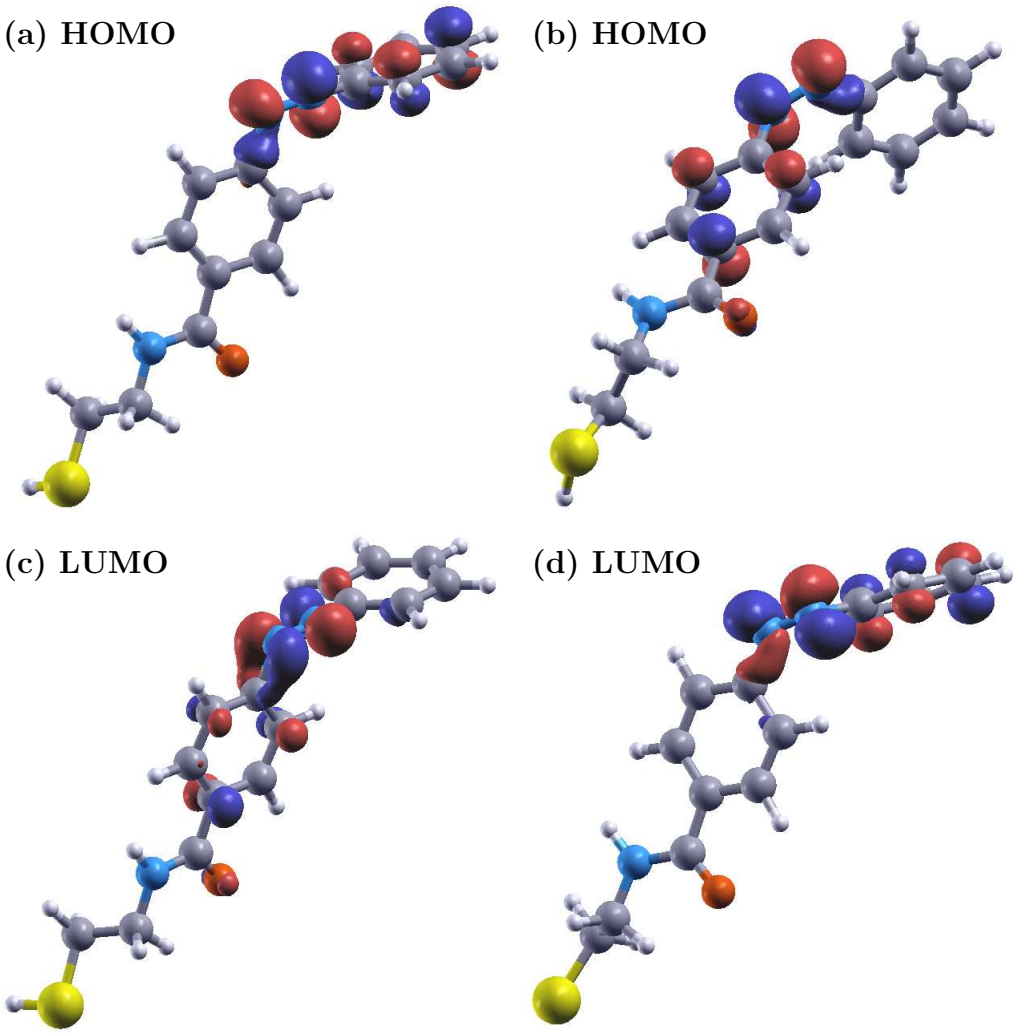


Figure 5.5: PBE/DZP frontier orbital diagrams of the transition state structures for gas phase AB. Panels (a) and (c) show the inversion transition state and panels (b) and (d) show the rotation transition state. C, H, N, O and S atoms are grey, white, blue, red and yellow, respectively.

The inversion and rotation energy profiles for adsorbed AB are illustrated in Figure 5.6, and the energy barriers are given in Table 5.3. For the neutral species, both isomerization channels have comparable activation energies. The activation energy decreases by 0.27 eV and 0.44 eV for the inversion and rotation pathways, respectively, for cationic adsorbed AB. The barrier for the rotation mechanism was lowered even more in comparison to the inversion mechanism for anionic adsorbed AB. The relative transition state stabilization for adsorbed AB species is not as large in comparison to the gas phase. This is due to the excess charge being partially delocalized in the gold surface. In other words, a significant portion of the HOMO and LUMO of the transition state is located within the surface, as was the case for the trans and cis isomers (Figure 5.4).

**Adsorbed Phase.** The addition of a positive or negative charge to AB adsorbed on a gold surface results in a decrease in the energy of activation for isomerization, thereby facilitating molecular switching. However, these energies are still far greater than the thermal energy. Furthermore, the resonance lifetimes of a charged state for an adsorbed molecule are generally short-lived (on the order of ps up to ns) [110-112], meaning that the timescale of the isomerization pathway may not be long enough to allow the entire mechanism to proceed through an ionic state. The distance of the azo group of AB from the surface, however, is expected to increase the lifetime from those of small molecules. In order for switching to occur more readily, one should consider the addition of substituents to either phenyl ring which may stabilize the transition state relative to the trans isomer.

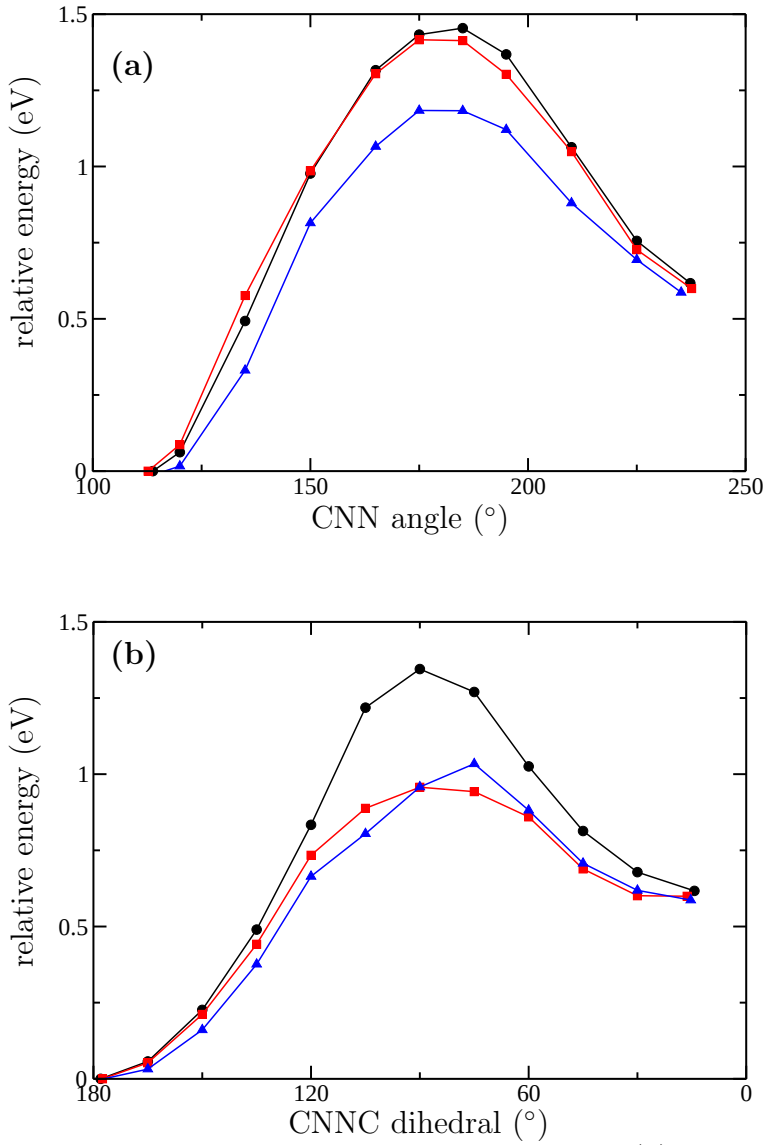


Figure 5.6: Energy profile of trans-cis isomerization of the (a) inversion and (b) rotation pathway for adsorbed AB. Black circles,red squares and blue triangles represent neutral, anionic and cationic species, respectively. All energies are relative to the energy of the optimized trans structure for that species. The anionic and cationic plots are translated up and down, respectively, such that the trans isomer had an energy of zero. The neutral and cationic adsorbed AB energies were calculated in the presence of a +1 V/nm electric field normal to the surface. The anionic adsorbed AB energies were determined in the presence of a -1 V/nm electric field normal to the surface. Lines are included only for clarity.

## 5.5 Summary

The behavior of chemisorbed AB under STM conditions (electric fields and tunnelling electrons) was examined computationally. Application of an electric field did not result in molecular switching in the zero-density, single molecule limit since the parallel trans geometry was favored at all field strengths (except at extreme fields). Determining ionic states of adsorbed AB was challenging due to surface effects, but was overcome by incorporating an electric field and using a small surface. Even with these considerations, orbitals of adsorbed AB were still found to be located partially within the surface. Isomerization energy barriers were lowered for both inversion and rotation pathways for cationic molecules, whereas only the rotational barrier was lowered substantially for anionic molecules.

# Chapter 6

# Conclusions

Chemisorbed azobenzene structures, whether in mixed monolayers or in zero-density regions, show promise in a number of areas from molecular electronics to biosensors. However, studies involving field- or electron tunnelling-induced switching are still at an exploratory stage. From a theoretical perspective, these systems are challenging: a large number of atoms are necessary to accurately describe the monolayer, treatment of the interaction of the molecules with the field is required, dispersive interactions that influence molecular conformations complicate the potential energy surface, inclusion of a metallic surface is computationally expensive and charge states are susceptible to surface quenching.

The equilibrium between cis and trans isomers of AB in a mixed monolayer was investigated with regards to electric fields, monolayer density, tilt angles and substituents. In the range of electric fields examined, TAB was found to be more prevalent than cis in the monolayer. Both TAB and CAB are highly polarizable molecules, but TAB being a planar molecule TAB being a planar molecule with extended conjugation through the azo group is more polarizable than CAB. The interplay between the permanent dipole coupling and polarizability contributions is such that at pos-

itive fields and strong negative fields, TAB dominates the monolayer composition. CAB was found, but not dominantly, at small to intermediate negative fields, with an optimal field strength of -0.9 V/nm. Neglecting polarizability lead to an incorrect interpretation of dipole-field coupling, resulting in CAB being favored at strong negative field strengths.

Density effects are also complex. The percentage of TAB in the monolayer increased as the density increased. It has been suggested that the availability of free volume for CAB is important in AB switching. However, for densities more than sufficiently small to accommodate CAB, repulsive interactions were not a factor. Rather, lateral interactions within the monolayer were found to influence density-dependent switching. TAB has a more similar geometry as the host alkylthiol matrix and, as a result, is able to pack more efficiently. The effect of the AB geometry and substituents were also addressed and found to influence AB switching behavior.

The tilt angle of AB was varied to account for different orientations within the monolayer. Because changing the tilt angle causes changes in dipole moments along $z$, attractive interactions and repulsive interactions, the field- and density-dependence on AB switching also changed. Larger tilt angles inhibit switching primarily due to more favorable TAB-$C_{12}$ lateral interactions and shift the optimal switching field strength due to different permanent dipole moment and polarizability orientations. Substituent effects were analyzed by varying adsorption and isomerization energies. Not surprisingly, more negative CAB adsorption energies and smaller isomerization energies promoted switching.

In the zero-density limit, DFT calculations, which include a Au(111)surface large enough to provide a substrate for the entire molecule, showed that AB was found to adopt two types of structures for the trans isomer and three types of structures for the cis isomer. The parallel geometries were found to be the lowest energy con-

formations for each isomer sincet hese structures maximize $\pi$-d interactions with the gold surface. Partial or full desorption costs a high energetic price, within 1-3 eV. Interactions between the amide group and the surface provide a large percentage of the binding energy. However, it competes with having to remain conjugated with the azobenzene moiety in determining the most effective binding geometry. Replacing the amide group with a more flexible ethyl group resulted in resulted in changes in two equilibrium geometries. Upright trans-AB adopted a larger tilt angle and semiparallel cis-AB had its phenyl ring closest to the butyl group lie fully parallel to the surface.

Two isomerization pathways were examined for parallel AB geometries in the electronic ground state. The inversion pathway was determined by increasing the CNN bond angle whereas the rotation pathway was calculated by making changes to the CNNC dihedral. For the parallel mechanism, the surface significantly affects the transition state structures, and the barriers for the two channels remain within the range calculated for analogous gas-phase isomerizations.

Field effects were also studied at the single molecule level using SIESTA. Within the -3 to +3 V/nm range, the most thermodynamically-favorable structures were the parallel geometries for each isomer. At a large field strength of 5 V/nm, upright TAB was favored. Applying an electric field did not result in any geometrical changes for parallel TAB nor parallel or semiparallel CAB, but the tilt angle did vary for upright structures. At high positive and negative fields, the tilt angle decreased resulting in taller structures.

Computational methods for determining charged states of chemisorbed AB were difficult since the molecular orbitals fall within the conduction band of the gold surface. Addition of an electric field, in combination to using a smaller surface, was necessary to have a component of the HOMO and LUMO localized on the adsorbed AB molecule. Without an electric field, or if a larger surface is used, frontier orbitals

are completely delocalized within the surface. Cationic AB in the gas phase showed a reduction in the isomerization energy in comparison to the neutral species. This was attributed to a decrease in the repulsion between nitrogen lone pairs of the cis isomer. This reduction was not nearly as large for the adsorbed, upright molecule due to a significant portion of the HOMO present on the surface. The isomerization energy of negatively-charged AB increased in the gas phase but decreased slightly in the adsorbed phase.

Inversion and rotation pathways for gas phase and upright, adsorbed AB were also studied. Frontier orbitals of both transition states were found to have antibonding character in the N=N bond region, although to varying degrees. Addition of a positive charge decreased the energy barrier for both pathways in comparison to the neutral species, while addition of a negative charge only decreased the rotational barrier. Gas phase barriers decreased more in the ionic state than adsorbed, upright barriers since the HOMO and LUMO are localized in the azobenzene moiety.

**Future Work.** While significant insight on the switching behavior of azobenzene on Au(111) has been gained in this thesis, there are more studies that could be performed on monolayer systems or at the zero-density limit. The statistical thermodynamics formalism could applied to a alkylthiol monolayer embedded with the butyl azobenzene derivative described in Section 4.2, which would confirm whether or not the phenyl ring orientation is responsible for the field-dependent switching. Also, temperature effects could be examined. At higher temperatures entropy becomes more important and, therefore, should lead to a greater amount of CAB in the monolayer. DFT calculations could be expanded to include physisorbed molecules that do not contain thiol linking groups. Another structure that could be analyzed is an azobenzene dimer. Azobenzene dimers stack together through their $\pi$-system, so there may be competition between molecule-molecule interactions and surface-molecule in-

teractions. Furthermore, energetics of a chemisorbed azobenzene molecule located at the edge of a monolayer can be determined through either DFT or molecular dynamics. Whether or not the upright structure is favored over the parallel structure would provide insight into what type of switching occurs at these locations in the monolayer.

# Bibliography

[1] Taveggia, C.; Zanazzi, G.; Petrylak, A.; Yano, H.; Rosenbluth, J.; Einheber, S.; Xu, X.; Esper, R. M.; Loeb, J. A.; Shrager, P.; Chao, M. V.; Falls, D. L.; Role, L.; Salzer, J. L. *Neuron* **2005,** *47,* 681.

[2] Mandal, M.; Breaker, R. R. *Nature Rev. Molec. Cell Bio.* **2004,** *5,* 451.

[3] Milburn, M. V.; Tong, L.; Devos, A. M.; Brunger, A.; Yamaizumi, Z.; Nishimura, S.; Kim, S. H. *Science* **1990,** *247,* 939.

[4] Lu, Y. L.; Nakano, M.; Ikeda, T. *Nature* **2003,** *425,* 145.

[5] Hugel, T.; Holland, N. B.; Cattani, A.; Moroder, L.; Seitz, M.; Gaub, H. E. *Science* **2002,** *296,* 1103.

[6] Oosaki, S.; Hayasaki, H.; Sakurai, Y.; Yajima, S.; Kimura, K. *Chem. Commun.* **2005,** 5226.

[7] Yager, K. G.; Barrett, C. J. *J. Photochem. Photobiol., A* **2006,** *182,* 250.

[8] Dietrich, P.; Michalik, F.; Schmidt, R.; Gahl, C.; Mao, G.; Breusing, M.; Raschke, M.; Priewisch,; Elsasser, T.; Mendelsohn, R.; Weinelt, M.; Rueck-Braun, K. *Appl. Phys. A* **2008,** *93,* 285.

[9] Horie, M.; Sakano, T.; Osakada, K.; Nakao, H. *Organometallics* **2004,** *23,* 18.

[10] Liu, N.; Chen, Z.; Dunphy, D. R.; Jiang, Y.-B.; Assink, R. A.; Brinker, C. J. *Angew. Chem.* **2000,** *115,* 1847.

[11] Liu, Z. F.; Hashimoto, K.; Fujishima, A. *Nature* **1990,** *347,* 658.

[12] Ikeda, T.; Tsutsumi, O. *Science* **1995,** *268,* 1873.

[13] Kawata, S.; Kawata, Y. *Chem. Rev.* **2000,** *100,* 1777.

[14] Harvey, A. J.; Abell, A. D. *Tetrahedron* **2000,** *56,* 9763.

[15] P. R. Westmark, J. P. K.; Smith, B. D. *J. Am. Chem. Soc.* **1993,** *115,* 3416.

[16] Natansohn, A.; Rochon, P. *Chem. Rev.* **2002,** *102,* 4139.

[17] Ichimura, K. *Chem. Rev.* **2000,** *100,* 1847.

[18] Kumar, A.; Ye, T.; Takami, T.; Yu, B.-C.; Flatt, A. K.; Tour, J. M.; Weiss, P. S. *Nano Lett.* **2008,** *8,* 1644.

[19] Zhang, X.; Wen, Y.; Li, Y.; Du, S.; Guo, H.; Yang, L.; Jiang, L.; Gao, H.; Song, Y. *J. Phys. Chem. C* **2008,** *112,* 8288.

[20] Zhang, C.; Du, M.-H.; Cheng, H.-P.; Zhang, X.-G.; Roitberg, A. E.; Krause, J. L. *Phys. Rev. Lett.* **2004,** *92,* 1583011.

[21] Tamai, N.; Miyasaka, H. *Chem. Rev.* **2000,** *100,* 1875.

[22] Cattaneo, P.; Persico, M. *Phys. Chem. Chem. Phys.* **1999,** *1,* 4739.

[23] Ishikawa, T.; Noro, T.; Shoda, T. *J. Chem. Phys.* **2001,** *115,* 7503.

[24] Cembran, A.; Bernardi, F.; Garavelli, M.; Gagliardi, L.; Orlandi, G. *J. Am. Chem. Soc.* **2004,** *126,* 3234.

[25] Diau, E. W.-G. *J. Phys. Chem. A* **2004,** *108,* 950.

[26] Zhu, Y.; Pu, M.; Fang, D.-C.; Ji, Y.-Q.; He, J.; Evans, D. G. *Struct. Chem.* **2010,** *21,* 817.

[27] Ootani, Y.; Satoh, K.; Nakayama, A.; Noro, T.; Taketsugu, T. *J. Chem. Phys.* **2009,** *131,* 194306.

[28] Tiago, M. L.; Ismail-Beigi, S.; Louie, S. G. *J. Chem. Phys.* **2005,** *122,* 094311.

[29] Wang, L.; Wang, X. *J. Molec. Structure: THEOCHEM* **2007,** *806,* 179.

[30] Klug, R. L.; Burcl, R. *J. Phys. Chem. A* **2010,** *114,* 6401.

[31] Ikegami, T.; Kurita, N.; Sekino, H.; Ishikawa, Y. *J. Phys. Chem. A* **2003,** *107,* 4555.

[32] Sokalski, W. A.; Gora, R. W.; Bartkowiak, W.; Kobylinski, P.; Sworakowski, J. *J. Chem. Phys.* **2001,** *114,* 5504.

[33] Crecca, C. R.; Roitberg, A. E. *J. Phys. Chem. A* **2006,** *110,* 8188.

[34] Fuchsel, G.; Klamroth, T.; Dokic, J.; Saalfrank, P. *J. Phys. Chem. B* **2006,** *110,* 16337.

[35] Elbing, M.; Błaszcyk, A.; von Hänish, C.; Mayor, M.; Ferri, V.; Grave, C.; Rampi, M. A.; Pace, G.; Samorì, P.; Shaporenko, A.; Zharnikov, M. *Adv. Funct. Mater.* **2008,** *18,* 2972.

[36] Weidner, T.; Bretthauer, F.; Ballav, N.; Motschmann, H.; Orendi, H.; Bruhn, C.; Siemeling, U.; Zharnikov, M. *Langmuir* **2008,** *24,* 11691.

[37] Evans, S. D.; Johnson, S. R.; Ringsdorf, H.; Williams, L. M.; Wolf, H. *Langmuir* **1998,** *14,* 6436.

[38] Hagen, S.; Kate, P.; Leyssner, F.; Nandi, D.; Wolf, M.; Tegeder, P. *J. Chem. Phys.* **2008,** *129,* 164102.

[39] Levy, N.; Comstock, M. J.; Cho, J.; Berbil-Bautista, L.; Kirakosian, A.; Lauterwasser, F.; Poulsen, D. A.; Fréchet, J. M. J.; Crommie, M. F. *Nano Lett.* **2009,** *9,* 935.

[40] Comstock, M. J.; Levy, N.; Kirakosian, A.; Cho, J.; Lauterwasser, F.; Harvey, J. H.; Strubbe, D. A.; Fréchet, J. M. J.; Trauner, D.; Louie, S. G.; Crommie, M. F. *Phys. Rev. Lett.* **2007,** *99,* 038301.

[41] Morgenstern, K. *Acc Chem. Res.* **2009,** *42,* 213.

[42] Henzl, J.; Mehlhorn, M.; Gawronski, H.; Rieder, K.; Morgenstern, K. *Angew. Chem. Int. Ed.* **2006,** *45,* 603.

[43] Smaali, K.; Lenfant, S.; Karpe, S.; Ocafrain, M.; Blanchard, P.; Deresmes, D.; Godey, S.; Rochefort, A.; Roncali, J.; Vuillaume, D. *ACS Nano* **2010,** *4,* 2411.

[44] Piantek, M.; Miguel, J.; Kruger, A.; Navio, C.; Bernien, M.; Ball, D. K.; Hermann, K.; Kuch, W. *J. Phys. Chem.* **2009,** *113,* 20307.

[45] Pace, G.; v. Ferri,; Grave, C.; Elbing, M.; von Hanisch, C.; Zharnikov, M.; Mayor, M.; Rampi, M. A.; Samori, P. *Proc. Natl. Acad. Sci.* **2007,** *104,* 9937.

[46] Lewis, P. A.; Inman, C. E.; Yao, Y.; Tour, J. M.; Hutchison, J. E.; Weiss, P. S. *J. Am. Chem. Soc.* **2004,** *126,* 12214.

[47] Yasuda, S.; Nakamura, T.; Matsumoto, M.; Shigekawa, H. *J. Am. Chem. Soc.* **2003,** *125,* 16430.

[48] Alemani, M.; Peters, M. V.; Hecht, S.; Rieder, K.-H.; Moresco, F.; Grill, L. *J. Am. Chem. Soc.* **2008,** *128,* 14446.

[49] Das, B.; Abe, S. *J. Phys. Chem. B* **2006,** *110,* 4247.

[50] Donhauser, Z. J.; Mantooth, B. A.; Kelly, K. F.; Bumm, L. A.; Monnell, J. D.; Stapleton, J. J.; Jr., D. W. P.; Rawlett, A. M.; Allara, D. L.; Tour, J. M.; Weiss, P. S. *Science* **2001,** *292,* 2303.

[51] Rochefort, A.; Ventra, M. D.; Avouris, P. *App. Phys. Lett.* **2001,** *78,* 2521.

[52] Emberly, E. G.; Kirczenow, G. *Phys. Rev. Lett.* **2003,** *91,* 188301.

[53] Katsonis, N.; Lubomska, M.; Pollard, M. M.; Feringa, B. L.; Rudolf, P. *Prog. Surf. Sci.* **2007,** *82,* 407.

[54] Henzl, J.; Bredow, T.; Morgenstern, K. *Chem. Phys. Lett.* **2007,** *435,* 278.

[55] Choi, B.; Khahng, S.; Kim, S.; Kim, H.; Kim, H. W.; Song, Y. J.; Ihm, J.; Kuk, Y. *Phys. Rev. Lett.* **2006,** *96,* 156106.

[56] Chandler, D. Introduction to Modern Statistical Mechanics. In ; Oxford University Press, Inc.: New York, 1987.

[57] McQuarrie, D. A. Statistical Mechanics. In ; Harper Collins Publishers, Inc.: New York, 1976.

[58] Hill, T. An Introduction to Statistical Mechanics. In ; Dover Publications, Inc.: New York, 1986.

[59] Cotter, M. A.; Wacker, D. C. *Phys. Rev. A* **1978,** *18,* 2669.

[60] Gelbart, W. M.; Gelbart, A. *Mol. Phys.* **1977,** *33,* 1387.

[61] Ren, C.-L.; Nap, R. J.; Szleifer, I. *J. Phys. Chem. B* **2008,** *112,* 16238.

[62] Carignano, M.; Szleifer, I. *Adv. Chem. Phys.* **1996,** *94,* 165.

[63] Szleifer, I.; Carignano, M. *J. Chem. Phys.* **1993,** *98,* 5005.

[64] Fang, F.; Szleifer, I. *Proc. Natl. Acad. Sci.* **2006,** *103,* 5769.

[65] Yaliraki, S. N.; Longo, G.; Gale, E.; Szleifer, I.; Ratner, M. A. *J. Chem. Phys.* **2006,** *125,* 074708.

[66] Gelbart, W. M.; Baron, B. A. *J. Chem. Phys.* **1977,** *66,* 207.

[67] Cotter, M. A. *J. Chem. Phys.* **1977,** *66,* 4710.

[68] Nogues, C.; Lang, P. *Langmuir* **2007,** *23,* 8385.

[69] Ulman, J. E. E.; Tillman, N. *Langmuir* **1989,** *5,* 1147.

[70] Riposan, A.; Liu, G. *J. Phys. Chem. B* **2006,** *110,* 23926.

[71] Tian, Y.; Umemura, J.; Takenaka, T. *Langmuir* **1988,** *4,* 1064.

[72] Mani, A. A.; Schultz, Z. D.; Champagne, B.; Humbert, C.; Dreesen, L.; Gewirth, A. A.; White, J. O.; Thiry, P. A.; Peremans, A.; Caudano, Y. *App. Surf. Sci.* **2004,** *237,* 444.

[73] "NAG Fortran Library Manual", 2008.

[74] Jensen, F. Introduction to Computational Chemistry. In ; John Wiley and Sons Ltd.: New York, 2007.

[75] Hohenberg, P.; Kohn, W. *Phys. Rev. B* **1964,** *136,* B864.

[76] Peverati, R.; Baldridge, K. K. *J. Chem. Theory Comput.* **2010,** *6,* 1924.

[77] Grimme, S.; Antony, J.; Ehrlich, S.; Krieg, H. *J. Chem. Phys.* **2010,** *132,* 154104.

[78] Vydrov, O. A.; van Voorhis, T. *J. Chem. Phys.* **2008,** *130,* 104105.

[79] Sanchez-Portal, D.; Ordejon, P.; Artacho, E.; Soler, J. M. *Int. J. Quantum Chem.* **1997,** *65,* 453.

[80] Soler, J. M.; Artacho, E.; Gale, J. D.; Carcia, A.; Junquera, J.; Ordejon, P.; Sanchez-Portal, D. *J. Phys.: Condens Matter* **2002,** *14,* 2745.

[81] Perdew, J. P.; Burke, K.; Ernzerhof, M. *Phys. Rev. Lett.* **1996,** *77,* 3865.

[82] Troullier, N.; Martins, J. L. *Phys. Rev. B* **1991,** *43,* 1993.

[83] Mercurio, G.; McNellis, E. R.; Martin, I.; Hagen, S.; Leyssner, F.; Soubatch, S.; Meyer, J.; Wolf, M.; Tegeder, P.; Tautz, F. *Phys. Rev. Lett.* **2010,** *104,* 036102.

[84] DiLavio, G. A.; Wolkow, R. A.; Johnson, E. R. *J. Chem. Phys.* **2005,** *122,* 044708.

[85] Mavrikakis, M.; Stoltze, P.; Norskov, J. K. *Catal. Lett.* **1991,** *43,* 1993.

[86] Samant, M. G.; Brown, C. A.; II, J. G. G. *Langmuir* **1992,** *8,* 1615.

[87] Bareman, J. P.; Klein, M. L. *J. Phys. Chem.* **1990,** *94,* 5202.

[88] Rappe, A. K.; Casewit, C. J.; Colwell, K. S.; Goddard, W. A.; Skiff, W. M. *J. Am. Chem. Soc.* **1992,** *128,* 1959.

[89] Lorentz, H. A. *Ann. Phys.* **1881,** *12,* 127.

[90] Berthelot, D. *Comptes Rendus de l'Académie des Sciences Paris* **1889,** *126,* 1703.

[91] Kong, J. *et al. J. Comput. Chem.* **2000,** *21,* 1532.

[92] Zwanzig, R. *J. Chem. Phys.* **1963,** *39,* 1714.

[93] Zehner, R. W.; Sita, L. R. *Langmuir* **1997,** *13,* 2973.

[94] Dhirani, A. A.; Zehner, R. W.; Hsung, R. P.; Guyot-Sionnest, P.; Sita, L. R. *J. Am. Chem. Soc.* **1996,** *118,* 3319.

[95] Ehler, T. T.; Malmberg, N.; Noe, L. J. *J. Chem. Phys.* **1997,** *101,* 1268.

[96] Fenter, P.; Eberhardt, E.; Liang, K. S.; Eisenberger, P. *J. Chem. Phys.* **1997,** *106,* 1600.

[97] Alkis, S.; Jiang, P.; Wang, L.-L.; Roitberg, A. E.; Cheng, H.-P.; Karuse, J. L. *J. Phys. Chem. C* **2007,** *111,* 14743.

[98] Moore, A. M.; Dameron, A. A.; Mantooth, B. A.; Smith, R. K.; Fuchs, D. J.; Ciszek, J. W.; Maya, F.; Yao, Y.; Tour, J. M.; Weiss, P. W. *J. Am. Chem. Soc.* **2006,** *128,* 1959.

[99] Rong, H.-T.; Frey, S.; Yang, Y.-J.; Zharnikov, M.; Buck, M.; Wuhn, M.; Woll, C.; Helmchen, G. *Langmuir* **2001,** *17,* 1582.

[100] Schlenoff, J. B.; Li, M.; Ly, H. *J. Am. Chem. Soc.* **1995,** *117,* 12528.

[101] Chidsey, C. E. D.; Liu, G. Y.; Rowntree, P.; Scoles, G. J. *J. Chem. Phys.* **1989,** *91,* 4421.

[102] III, N. C.; Eisenberger, P.; Leung, T. Y. B.; Swartz, P.; Scoles, G.; Poirier, G. E.; Tarlov, M. J. *J. Chem. Phys.* **1994,** *101,* 11031.

[103] Poirier, G. E.; Tarlov, M. J.; Rushmeier, H. E. *Langmuir* **1994,** *10,* 3383.

[104] Jung, D. *Bull. Korean Chem. Soc.* **2001,** *22,* 499.

[105] McNellis, E. R.; Meyer, J.; Reuter, K. *Phys. Rev. B* **2009,** *80,* 205414.

[106] Jenkins, S. J. *Proc. R. Soc. London, Ser. A* **2009,** *465,* 2949.

[107] McNellis, E. R.; Bronner, C.; Meyer, J.; Weinelt, M.; Tegeder, P.; Reuter, K. *Phys. Chem. Chem. Phys.* **2010,** *12,* 6404.

[108] Tonigold, K.; Grob, A. *J. Chem. Phys.* **2010,** *132,* 224701.

[109] Bilic, A.; Reimers, J. R.; Hush, N. S.; Hoft, R. C.; Ford, M. J. *J. Chem. Theory Comput.* **2006,** *2,* 1093.

[110] Alavi, S.; Rousseau, R.; Patitsas, S. N.; Lopinski, G. P.; Wolkow, R. A.; Seideman, T. *Phys. Rev. Lett.* **2000,** *85,* 5372.

[111] Jorn, R.; Seideman, T. *J. Chem. Phys.* **2006,** *124,* 084703.

[112] Alavi, S.; Seideman, T. *J. Chem. Phys.* **2001,** *115,* 1882.

# Appendix A

# Additional Information

### A.0.1 Helmholtz Free Energy

The attractive interaction parameter described in Section 3.2 was calculated using the Fortran program shown in Figure A.1. Permanent dipole moments and polarizabilities were rotated using the Fortran program shown in Figure A.2. The Helmholtz free energy expression was optimized numerically as a function of the mole fraction of TAB. This was accomplished using the program shown in Figure **??**.

### A.0.2 DFT Calculations

All DFT optimizations were given the input parameters shown in Figure A.4, except with different initial geometries for the azobenzene molecule. The molecular coordinates were entered in the form of a $Z$-matrix because it allowed for simple alteration of the CNN bond angle and CNNC dihedral. A maximum of 1000 conjugate gradient (CG) steps was allowed, but calculations reaching this number did not reach a stable energy and, consequently, were not reported.

The utility program DENCHAR was used with the following method. First,

SIESTA was run with WriteDenchar and WriteDM set to true, KgridCutoff set to 10 Å and a WaveFuncKpoint block added. Files ending in PLD, DIM, DM, WFS and ion were transfered to a different directory along with the DENCHAR executable. The DENCHAR input file is shown in Figure A.5. It is important to ensure that there is sufficient space between the minimum (maximum) coordinate of the SIESTA structure and the minimum (maximum) coordinate specified in the DENCHAR input file. Once DENCHAR is compiled and run, orbitals and electron density can be viewed with xcrysden by opening a cube file.

```
implicit real*8(a-h,o-z)
character xyzfile*50,potfile*50,attp1*2,attp*2,ptp*2
parameter (np=2,natmax=10000,natpm=1000)
dimension x(np,natmax),y(np,natmax),z(np,natmax),attp(np,natmax)
dimension x1(natmax),y1(natmax),z1(natmax),attp1(natmax)
dimension ptp(natpm),xp(natpm),dp(natpm)
dimension dpij(natpm,natpm),xp6(natpm,natpm)
dimension kattp(np,natmax)
dimension nat(2)
common/dipole/uax,uay,uaz,ubx,uby,ubz

open(unit=10,file='inppot')

 write (*,*) 'enter u1x,u1y,u1z in D'
 read (*,*) uax,uay,uaz
 write (*,*) 'enter u2x,u2y,u2z in D'
 read (*,*) ubx,uby,ubz


do i=1,np
 read(10,*)xyzfile
 write(*,*)xyzfile
 call xyzread(xyzfile,nat(i),attp1,x1,y1,z1)
 do j=1,nat(i)
  attp(i,j)=attp1(j)
  x(i,j)=x1(j)
  y(i,j)=y1(j)
  z(i,j)=z1(j)
 enddo
enddo

read(10,*)potfile
write(*,*)potfile
read(10,*)nsteps,dr

open(unit=15,file='uff.params')
read(15,*)npar
do i=1,npar
 read(15,*)ptp(i),xp(i),dp(i)
enddo
do i=1,npar
 do j=1,npar
  xpij=(xp(i)+xp(j))/2.0d0
  dpij(i,j)=dsqrt(dp(i)*dp(j))
  xp2=xpij*xpij
  xp4=xp2*xp2
  xp6(i,j)=xp4*xp2
 enddo
enddo
```

```
do i=1,np
 do j=1,nat(i)
  do k=1,npar
   if(attp(i,j).eq.ptp(k))kattp(i,j)=k
  enddo
 enddo
enddo
call integrate(dr,nsteps,np,nat,x,y,z,xp6,dpij,attp,kattp,potfile)

end

subroutine integrate(dr,nsteps,np,nat,x,y,z,xp6,dp,attp,
1      kattp,potfile)
implicit real*8(a-h,o-z)
character potfile*(*),attp*(*)
parameter (natmax=10000,natpm=1000)
dimension x(np,natmax),y(np,natmax),z(np,natmax)
dimension x2(natmax),y2(natmax),z2(natmax)
dimension x3(natmax),y3(natmax),z3(natmax)
dimension xp6(natpm,natpm),dp(natpm,natpm),nat(np)
dimension kattp(np,natmax),d(nsteps)
dimension attp(np,natmax)
open(unit=26,file=potfile)
vint=0.0d0
voldk=1000.0d0
v=1000.0d0
k=0
pi=4.0d0*datan(1.0d0)
dangle=pi/180.0d0
cd=dcos(dangle)
sd=dsin(dangle)
do jangle=1,360
print*,x(2,1),y(2,1)
do i=1,nat(2)
 y2(i)=y(2,i)
 x2(i)=x(2,i)
 y3(i)=y(2,i)
 x3(i)=x(2,i)
enddo
do js=-nsteps,nsteps
 call slide(nat(2),y3,y2,dr,js)
 do i=1,nat(2)
  y(2,i)=y2(i)
 enddo
 do is=-nsteps,nsteps
  volder=voldk
  voldk=v
  vold=v
```

```
        call slide(nat(2),x3,x2,dr,is)
         do i=1,nat(2)
          x(2,i)=x2(i)
         enddo
         d(is)=dsqrt((x(2,1)-x(1,1))**2+(y(2,1)-y(1,1))**2)
         call potent(is,np,nat,x,y,z,xp6,dp,kattp,v)
ctest!
c        d2=d(is)*d(is)
c        d6=d2*d2*d2
c        d12=d6*d6
c        v=(1.0d0/d12)-(1.0d0/d6)
         if(js.eq.0.and.x(2,1).gt.x(1,1))write(17,500)d(is),v,x(2,1)
c        print*,js,is,x(2,1),y(2,1),v
ctest!
         write(26,500)d(is),v
c        if(k.eq.0.and.voldk.le.0.0d0.and.voldk.le.volder.
c    1     and.voldk.le.v)then
c        if(k.eq.0.and.voldk.le.0.0d0.and.volder.gt.0.0d0.
c    1     and.voldk.ge.v)then
c         sigma=d(is-1)
c         do i=1,np
c          do j=1,nat(i)
c           write(28,510)attp(i,j),x(i,j),y(i,j),z(i,j)
c          enddo
c         enddo
c         k=1
c         print*,'sigma',d(is-1),v
c        endif
         if(v.le.0.0d0)then
          vint=vint+v*dr*dr
c        print*,js,is,v,vint
         endif
        enddo
       enddo
       write(*,*)vint
500    format(' ',10f14.7)
510    format(' ',a5,10f14.7)
       return
       end


       subroutine slide(nat,x1,x,d,k)
       implicit real*8(a-h,o-z)
       dimension x(nat),x1(nat)
       do i=1,nat
        x(i)=x1(i)+d*k
       enddo
       return
       end
```

```
      subroutine rotate(nat,x,y,cd,sd)
      implicit real*8(a-h,o-z)
      dimension x(nat),y(nat)
      do i=1,nat
       x(i)=x(i)*cd
       y(i)=y(i)*sd
      enddo
      return
      end


      subroutine potent(is,np,nat,x,y,z,xp6,dp,kattp,v)
      implicit real*8(a-h,o-z)
      parameter (natmax=10000,natpm=1000)
      dimension x(np,natmax),y(np,natmax),z(np,natmax)
      dimension xp6(natpm,natpm),dp(natpm,natpm)
      dimension kattp(np,natmax),nat(np)
      common/dipole/uax,uay,uaz,ubx,uby,ubz

      v=0.0d0
      do i=1,nat(1)
       ka1=kattp(1,i)
       x1=x(1,i)
       y1=y(1,i)
       z1=z(1,i)
       do j=1,nat(2)
        ka2=kattp(2,j)
        xp6l=xp6(ka1,ka2)
        dpl=dp(ka1,ka2)
        xp12=xp6l*xp6l
c       print*,i,j,ka1,ka2 !
        x2=x(2,j)
        y2=y(2,j)
        z2=z(2,j)
        rxij=x2-x1
        ryij=y2-y1
        rzij=z2-z1
        rij2=rxij*rxij+ryij*ryij+rzij*rzij
        if (i.eq.1) then
         if (j.eq.1) then
          rNNx=rxij
          rNNy=ryij
          rNNz=rzij
          rNN2=rij2
         endif
        endif
        if(rij2.lt.0.00010d0)then
         v=1000000000000.0d0
```

```
        else
         rij4=rij2*rij2
         rij6=rij4*rij2
         rij12=rij6*rij6
c        print*,'h',i,j,rij12
         term1=xp12/rij12
         term2=2.0d0*xp6l/rij6
         vinstant=(term1-term2)*dpl
         v=v+vinstant
c        if(is.gt.5000.and.i.eq.33)then
c            write(*,500)is,i,j,rij2,vinstant,v
c        endif
        endif
       enddo
      enddo
      eps=14.39326d0
      dpl1=(uax*ubx+uay*uax+uaz*ubz)
      dpl2=3*(uax*rNNx+uay*rNNy+uaz*rNNz)*(ubx*rNNx+uby*rNNy+ubz*rNNz)
      vdipole=1/eps*(dpl1/rNN2**1.50d0-dpl2/rNN2**2.50d0)
      v=v+vdipole
500   format(' ',3i7,10f12.5)
c     write (*,*) v
      return
      end


      subroutine xyzread(xyzfile,nat,attp,x,y,z)
      implicit real*8(a-h,o-z)
      character xyzfile*(*),attp*2
      integer xyzunit
      parameter (xyzunit=25,natmax=10000)
      dimension x(natmax),y(natmax),z(natmax),attp(natmax)
c     print*,'in'
      open(unit=xyzunit,file=xyzfile)
      read(xyzunit,*)nat
c     print*,nat
      read(xyzunit,*)
      do i=1,nat
       read(xyzunit,*)attp(i),x(i),y(i),z(i)
c      print*,i,attp(i)
      enddo
      close(xyzunit)
c     print*,'closed'
      do i=1,nat
       if(attp(i).eq.'S')then
       zslide=z(i)
c      print*,'S is atom',i,zslide
       endif
      enddo
      do i=1,nat
       z(i)=z(i)-zslide
c      print*,i,x(i),y(i),z(i)
      enddo
```

```
        else
         rij4=rij2*rij2
         rij6=rij4*rij2
         rij12=rij6*rij6
c        print*,'h',i,j,rij12
         term1=xp12/rij12
         term2=2.0d0*xp6l/rij6
         vinstant=(term1-term2)*dpl
         v=v+vinstant
c        if(is.gt.5000.and.i.eq.33)then
c            write(*,500)is,i,j,rij2,vinstant,v
c        endif
        endif
       enddo
      enddo
      eps=14.39326d0
      dpl1=(uax*ubx+uay*uax+uaz*ubz)
      dpl2=3*(uax*rNNx+uay*rNNy+uaz*rNNz)*(ubx*rNNx+uby*rNNy+ubz*rNNz)
      vdipole=1/eps*(dpl1/rNN2**1.50d0-dpl2/rNN2**2.50d0)
      v=v+vdipole
500   format(' ',3i7,10f12.5)
c     write (*,*) v
      return
      end


      subroutine xyzread(xyzfile,nat,attp,x,y,z)
      implicit real*8(a-h,o-z)
      character xyzfile*(*),attp*2
      integer xyzunit
      parameter (xyzunit=25,natmax=10000)
      dimension x(natmax),y(natmax),z(natmax),attp(natmax)
c     print*,'in'
      open(unit=xyzunit,file=xyzfile)
      read(xyzunit,*)nat
c     print*,nat
      read(xyzunit,*)
      do i=1,nat
       read(xyzunit,*)attp(i),x(i),y(i),z(i)
c      print*,i,attp(i)
      enddo
      close(xyzunit)
c     print*,'closed'
      do i=1,nat
       if(attp(i).eq.'S')then
       zslide=z(i)
c      print*,'S is atom',i,zslide
       endif
      enddo
      do i=1,nat
       z(i)=z(i)-zslide
c      print*,i,x(i),y(i),z(i)
      enddo return end
```

Figure A.1: Fortran code to calculate the attractive interaction parameter.

```
program rotate
implicit none

integer natoms !number of atoms
integer atom !atom number
integer nmax !max number of atoms
parameter (nmax=1000)
real x(nmax),y(nmax),z(nmax) !original coordinates
real xrot(nmax),yrot(nmax),zrot(nmax) !rotated coordinates
character*1 element(nmax)
real a1,a2,a3,b1,b2,b3,c1,c2,c3 !rotation matrix coordinates
                                !a-c are rows, 1-3 are columns
real angle !angle in radians

!read original coordinates
open(unit=10,file='azo_trans_tilt_20.xyz')
read(10,*) natoms
read(10,*)
do atom=1,natoms
  read(10,*) element(atom),x(atom),y(atom),z(atom)
enddo
close(10)

angle=0.174532925

!rotate coordinates
a1=cos(angle)
a2=0.
a3=sin(angle)
b1=0.
b2=1.
b3=0.
c1=-sin(angle)
c2=0.
c3=cos(angle)
do atom=1,natoms
  xrot(atom)=a1*x(atom)+a2*y(atom)+a3*z(atom)
  yrot(atom)=b1*x(atom)+b2*y(atom)+b3*z(atom)
  zrot(atom)=c1*x(atom)+c2*y(atom)+c3*z(atom)
enddo

!write rotated coordinates
open(unit=20,file='azo_trans_tilt_10.xyz')
write(20,*) natoms
write(20,*)
do atom=1,natoms
  write(20,*) element(atom),xrot(atom),yrot(atom),zrot(atom)
enddo

end
```

Figure A.2: Fortran code to rotate molecular moments.

```
      program optimize
      implicit none
      !optimizes free energy of 3 component SAM, of which 2 components
      !are isomers of each other
      double precision dG !Gibbs free energy of isomerization in kJ/mol
      double precision c,d !minimum found within interval (c,d)
      double precision eps,t
      double precision f !free energy of SAM
      double precision g !1st derivative of free energy
      double precision x !mole fraction of one isomer (variable)
      double precision x_percent !% of isomer in trans configuration
      double precision y_percent !% of isomer in cis configuration
      integer ifail
      integer maxcal !max number of calls to energy
      double precision y !mole fraction of isomers (known)
      double precision temp !temp in K
      double precision beta !1/(Boltzmann*Na*T) in mol/kJ
      double precision rho !density of SAM in nm^-2
      double precision Vext !applied electric field strength in V/nm
      integer i,nmax
      parameter (nmax=100)
      double precision A(nmax) !attractive terms in kJ*nm^2/mol
      double precision B(nmax) !excluded volume terms in nm^2
      double precision h(nmax) !adsorption energies in kJ/mol
      double precision u(nmax) !z-component dipole moments in C*nm/mol
      double precision alpha(nmax) !z,z-component polarizability in C*nm^2/V*mol
      integer nA,nB,nh,nu,nalpha !number of A,B,h,u and alpha terms
      common/parameters/rho,beta,y,Vext,A,B,h,u,dG,alpha
      external funct !calculates function and 1st derivative values
      external e04bbf !NAG subroutine that finds minimum using function
                      !and first derivative values

      open (unit=10,file='attract_pot.dat')
      read (10,*) nA
      do i=1,nA
         read (10,100) A(i)
      enddo
100   format (1(F15.8))
      close (10)

      open (unit=20,file='exclud_vol.dat')
      read (20,*) nB
      do i=1,nB
         read (20,200) B(i)
      enddo
200   format (1(F15.8))
      close (20)

      open (unit=30,file='adsorption_E.dat')
      read (30,*) nh
      do i=1,nh
         read (30,100) h(i)
      enddo
```

```
300   format (1(F15.8))
      close (30)

      open (unit=40,file='z_dipole.dat')
      read (40,*) nu
      do i=1,nu
         read (40,100) u(i)
      enddo
400   format (1(F15.8))
      close (40)

      open (unit=50,file='alpha.dat')
      read (50,*) nalpha
      do i=1,nalpha
         read (50,100) alpha(i)
      enddo
500   format (1(F15.8))
      close (50)


      temp=298.0d0
      dG=24.2d0

      beta=120.27137/temp

      open(unit=60,file='p_tilt_30_-1.5.dat')

      do rho=0.001d0, 6.0005d0, 0.001d0
!      do Vext=-8.0005d0, 8.0005d0, 0.001d0
            eps=0.0d0
            t=0.0d0
            !eps and t are set to zero so that e04bbf will reset them
            !to default values
            y=0.01d0
!            rho=0.01d0
            Vext=-1.5d0
            c=0.0000000000001d0
            d=y-0.000000000010d0
            maxcal=50 !allow 50 calls to funct
            ifail=1

            call e04bbf (funct,eps,t,c,d,maxcal,x,f,g,ifail)

            x_percent=x/y*100.
            y_percent=100.-x_percent

            if (x_percent .gt. 0.1 .and. x_percent .lt. 99.9) then
               write (60,600) rho,x_percent
            endif
      enddo
600   format (3(F10.5))
      stop
      end
```

```
subroutine funct (xc,fc,gc)

double precision dG !Gibbs free energy of isomerization in kJ/mol
double precision xc !mole fraction of one isomer (variable)
double precision fc !free energy of SAM
double precision gc !1st derivative of free energy
double precision rho !density of SAM in nm^-2
double precision beta !1/(Boltzmann*Na*T) in mol/kJ
double precision Vext !applied electric field strength in V/nm
double precision y !mole fraction of isomers (known)
integer nmax
parameter (nmax=100)
double precision A(nmax) !attractive terms in kJ*nm^2/mol
double precision B(nmax) !excluded volume terms in nm^2
double precision h(nmax) !adsorption energies in kJ/mol
double precision u(nmax) !z-component dipole moments in C*nm/mol
double precision alpha(nmax) !z,z-component polarizability in C*nm^2/V*mol
common/parameters/rho,beta,y,Vext,A,B,h,u,dG,alpha

if (xc.eq.y) then
   xc=y
   return
endif

if(xc.eq.0) then
   xc=0
   return
endif

fc=rho*log(rho)
&   +rho*((1.-y)*log(1.-y)+xc*log(xc)+(y-xc)*log(y-xc))
&   +rho*beta*((1.-y)*h(1)+xc*h(2)+(y-xc)*h(3))
&   +rho**2.*beta*0.5*((1.-y)**2.*A(1)+xc*(1.-y)*(A(2)+A(4))
&                     +(y-xc)*(1.-y)*(A(3)+A(7))+xc**2.*A(5)
&                     +xc*(y-xc)*(A(6)+A(8))+(y-xc)**2.*A(9))
&   -rho*beta*Vext*((1.-y)*u(1)+xc*u(2)+(y-xc)*u(3))/1000
&   -rho*beta*Vext**2.*((1.-y)*alpha(1)
&                      +xc*alpha(2)+(y-xc)*alpha(3))/1000
&   -rho*log(1.-rho*0.5*((1.-y)**2.*B(1)+2.*xc*(1.-y)*B(2)
&                       +2.*(y-xc)*(1.-y)*B(3)+xc**2.*B(4)
&                       +2*xc*(y-xc)*B(5)+(y-xc)**2.*B(6)))
&   +rho*beta*dG*(y-xc)

    gc=rho*log(xc/(y-xc))
    &   +rho*beta*(h(2)-h(3))
    &   +rho**2.*beta*(0.5*(1.-y)*(A(2)+A(4))-0.5*(1.-y)*(A(3)+A(7))
    &                  +xc*A(5)+0.5*(y-2.*xc)*(A(6)+A(8))-(y-xc)*A(9))
    &   -rho*beta*Vext*(u(2)-u(3))/1000
    &   -rho*beta*Vext**2.*(alpha(2)-alpha(3))/1000
    &   +rho**2.*((1.-y)*B(2)-(1.-y)*B(3)+xc*B(4)
    &             +(y-2.*xc)*(B(5))-(y-xc)*B(6))
    &    /(1.-rho*0.5*((1.-y)**2.*B(1)+2.*xc*(1.-y)*B(2)
    &                  +2.*(y-xc)*(1.-y)*B(3)+xc**2.*B(4)
    &                  +xc*(y-xc)*(B(5)+B(6))+(y-xc)**2.*B(7)))
    &   -rho*beta*dG
     return
     end
```

Figure A.3: Fortran code to optimize the Helmholtz free energy.

```
SystemName          azo
SystemLabel         azo
NumberOfAtoms       162
NumberOfSpecies     6
LatticeConstant     1.0 Ang
%block LatticeVectors
   50.000000    0.0000000    0.0000000
   0.0000000   50.0000000    0.0000000
   0.0000000    0.0000000   50.0000000
%endblock LatticeVectors

%block ChemicalSpeciesLabel
 1  6  C      # Species index, atomic number, species label
 2  7  N
 3  8  O
 4  1  H
 5 16  S
 6 79  Au
%endblock ChemicalSpeciesLabel

%block ExternalElectricField
0.000 0.000 -0.100 V/Ang
%endblock ExternalElectricField

ZM.UnitsLength Ang
ZM.UnitsAngle deg
%block Zmatrix
molecule
 5   0    0   0  x1       y1       z1      1  1  1
 1   1    0   0  cs2      a1       a2      1  1  1
 1   2    1   0  cc3     ccs3      a3      1  1  1
 2   3    2   1  nc4     ncc4      var1      1  1  1
 4   4    3   2  hn5     hnc5      dih5      1  1  1
 1   4    3   2  cn6     cnc6      var2      1  1  1
 3   6    4   3  oc7     ocn7      dih7      1  1  1
 4   2    3   4  hc8     hcc8      dih8      1  1  1
 4   2    3   4  hc8     hcc9      dih9      1  1  1
 4   3    2   1  hc8     hcc10     dih10      1  1  1
 4   3    2   1  hc8     hcc11     dih11      1  1  1
 1   6    4   3  cc12    ccn12     var3      1  1  1
 1  12    6   4  cc13    ccc13     dih13      1  1  1
 1  13   12   6  cc14    ccc14     dih14      1  1  1
 1  14   13  12  cc15    ccc14     000.0      1  1  0
 1  15   14  13  cc16    ccc14     000.0      1  1  0
 1  12    6   4  cc17    ccc17     dih17      1  1  1
 4  17   12   6  hc18    hcc18     dih18      1  1  1
 4  16   17  12  hc18    hcc19     dih19      1  1  1
 4  14   13  12  hc18    hcc20     dih20      1  1  1
 4  13   12   6  hc18    hcc21     dih21      1  1  1
 2  15   14  13  nc22    ncc22     dih22      1  1  1
 2  22   15  14  nn23    nnc23     dih23      1  1  1
 1  23   22  15  cn24    cnn24     dih24      1  1  1
 1  24   23  22  cc25    ccn25     dih25      1  1  1
```

```
 1  25   24  23  cc26    ccc14     dih26      1  1  1
 1  26   25  24  cc27    ccc14     000.0      1  1  0
 1  27   26  25  cc28    ccc14     000.0      1  1  0
 1  24   23  22  cc29    ccn29     dih29      1  1  1
 4  29   24  23  hc18    hcc30     dih30      1  1  1
 4  28   29  24  hc18    hcc31     dih31      1  1  1
 4  27   26  25  hc18    hcc32     dih32      1  1  1
 4  26   25  24  hc18    hcc33     dih33      1  1  1
 4  25   24  23  hc18    hcc34     dih34      1  1  1
cartesian
6     -4.278661     -3.801158    -15.697404  0 0 0
6      7.133641     -3.801158    -15.697404  0 0 0
6      7.133641      6.320787    -15.697404  0 0 0
6     -4.278661      6.320787    -15.697404  0 0 0
6     -2.852260     -1.268393    -15.697571  0 0 0
6      8.560042     -1.268393    -15.697571  0 0 0
6      8.560042      8.853552    -15.697571  0 0 0
6     -2.852260      8.853552    -15.697571  0 0 0
6     -4.277020      1.260062    -15.697200  0 0 0
6      7.135282      1.260062    -15.697200  0 0 0
6      7.135282     11.382007    -15.697200  0 0 0
6     -4.277020     11.382007    -15.697200  0 0 0
6     -2.850979      3.792360    -15.697340  0 0 0
6      8.561323      3.792360    -15.697340  0 0 0
6      8.561323     13.914305    -15.697340  0 0 0
6     -2.850979     13.914305    -15.697340  0 0 0
6     -1.426245     -3.800232    -15.697621  0 0 0
6      9.986057     -3.800232    -15.697621  0 0 0
6      9.986057      6.321713    -15.697621  0 0 0
6     -1.426245      6.321713    -15.697621  0 0 0
6      0.000259     -1.269102    -15.697917  0 0 0
6     11.412561     -1.269102    -15.697917  0 0 0
6     11.412561      8.852843    -15.697917  0 0 0
6      0.000259      8.852843    -15.697917  0 0 0
6     -1.424600      1.261009    -15.697455  0 0 0
6      9.987702      1.261009    -15.697455  0 0 0
6      9.987702     11.382954    -15.697455  0 0 0
6     -1.424600     11.382954    -15.697455  0 0 0
6      0.001363      3.791936    -15.697688  0 0 0
6     11.413665      3.791936    -15.697688  0 0 0
6     11.413665     13.913881    -15.697688  0 0 0
6      0.001363     13.913881    -15.697688  0 0 0
6      1.425224     -3.799007    -15.697933  0 0 0
6     12.837526     -3.799007    -15.697933  0 0 0
6     12.837526      6.322938    -15.697933  0 0 0
6      1.425224      6.322938    -15.697933  0 0 0
6      2.851611     -1.268806    -15.698147  0 0 0
6     14.263913     -1.268806    -15.698147  0 0 0
6     14.263913      8.853139    -15.698147  0 0 0
6      2.851611      8.853139    -15.698147  0 0 0
6      1.426850      1.262449    -15.697837  0 0 0
6     12.839152      1.262449    -15.697837  0 0 0
6     12.839152     11.384394    -15.697837  0 0 0
```

```
6      1.426850     11.384394    -15.697837  0 0 0
6      2.852871      3.792156    -15.697807  0 0 0
6     14.265173      3.792156    -15.697807  0 0 0
6     14.265173     13.914101    -15.697807  0 0 0
6      2.852871     13.914101    -15.697807  0 0 0
6      4.278424     -3.798486    -15.698272  0 0 0
6     15.690726     -3.798486    -15.698272  0 0 0
6     15.690726      6.323459    -15.698272  0 0 0
6      4.278424      6.323459    -15.698272  0 0 0
6      5.706115     -1.267741    -15.698265  0 0 0
6     17.118417     -1.267741    -15.698265  0 0 0
6     17.118417      8.854204    -15.698265  0 0 0
6      5.706115      8.854204    -15.698265  0 0 0
6      4.280121      1.263037    -15.698086  0 0 0
6     15.692423      1.263037    -15.698086  0 0 0
6     15.692423     11.384982    -15.698086  0 0 0
6      4.280121     11.384982    -15.698086  0 0 0
6      5.707100      3.793272    -15.698180  0 0 0
6     17.119402      3.793272    -15.698180  0 0 0
6     17.119402     13.915217    -15.698180  0 0 0
6      5.707100     13.915217    -15.698180  0 0 0
6     -2.855539     -2.926923    -13.282747  0 0 0
6      8.556763     -2.926923    -13.282747  0 0 0
6      8.556763      7.195022    -13.282747  0 0 0
6     -2.855539      7.195022    -13.282747  0 0 0
6     -1.431867     -0.395965    -13.282786  0 0 0
6      9.980435     -0.395965    -13.282786  0 0 0
6      9.980435      9.725980    -13.282786  0 0 0
6     -1.431867      9.725980    -13.282786  0 0 0
6     -2.854196      2.134256    -13.282588  0 0 0
6      8.558106      2.134256    -13.282588  0 0 0
6      8.558106     12.256201    -13.282588  0 0 0
6     -2.854196     12.256201    -13.282588  0 0 0
6     -1.430453      4.664811    -13.282535  0 0 0
6      9.981849      4.664811    -13.282535  0 0 0
6      9.981849     14.786756    -13.282535  0 0 0
6     -1.430453     14.786756    -13.282535  0 0 0
6     -0.002640     -2.925626    -13.282851  0 0 0
6     11.409662     -2.925626    -13.282851  0 0 0
6     11.409662      7.196319    -13.282851  0 0 0
6     -0.002640      7.196319    -13.282851  0 0 0
6      1.422620     -0.394218    -13.282893  0 0 0
6     12.834922     -0.394218    -13.282893  0 0 0
6     12.834922      9.727727    -13.282893  0 0 0
6      1.422620      9.727727    -13.282893  0 0 0
6     -0.001431      2.135393    -13.282897  0 0 0
6     11.410871      2.135393    -13.282897  0 0 0
6     11.410871     12.257338    -13.282897  0 0 0
6     -0.001431     12.257338    -13.282897  0 0 0
6      1.424458      4.666564    -13.282991  0 0 0
6     12.836760      4.666564    -13.282991  0 0 0
6     12.836760     14.788509    -13.282991  0 0 0
6      1.424458     14.788509    -13.282991  0 0 0
```

```
6      2.849780     -2.925620    -13.283183  0 0 0
6     14.262082     -2.925620    -13.283183  0 0 0
6     14.262082      7.196325    -13.283183  0 0 0
6      2.849780      7.196325    -13.283183  0 0 0
6      4.273671     -0.394647    -13.283342  0 0 0
6     15.685973     -0.394647    -13.283342  0 0 0
6     15.685973      9.727298    -13.283342  0 0 0
6      4.273671      9.727298    -13.283342  0 0 0
6      2.850950      2.135655    -13.282990  0 0 0
6     14.263252      2.135655    -13.282990  0 0 0
6     14.263252     12.257600    -13.282990  0 0 0
6      2.850950     12.257600    -13.282990  0 0 0
6      4.275101      4.666140    -13.283009  0 0 0
6     15.687403      4.666140    -13.283009  0 0 0
6     15.687403     14.788085    -13.283009  0 0 0
6      4.275101     14.788085    -13.283009  0 0 0
6      5.702961     -2.925478    -13.283198  0 0 0
6     17.115263     -2.925478    -13.283198  0 0 0
6     17.115263      7.196467    -13.283198  0 0 0
6      5.702961      7.196467    -13.283198  0 0 0
6      7.128220     -0.393587    -13.283452  0 0 0
6     18.540522     -0.393587    -13.283452  0 0 0
6     18.540522      9.728358    -13.283452  0 0 0
6      7.128220      9.728358    -13.283452  0 0 0
6      5.704251      2.135542    -13.283166  0 0 0
6     17.116553      2.135542    -13.283166  0 0 0
6     17.116553     12.257487    -13.283166  0 0 0
6      5.704251     12.257487    -13.283166  0 0 0
6      7.129608      4.667439    -13.283131  0 0 0
6     18.541910      4.667439    -13.283131  0 0 0
6     18.541910     14.789384    -13.283131  0 0 0
6      7.129608     14.789384    -13.283131  0 0 0
variables
 x1           0.6099407132386246
 y1           0.8018464611629402
 z1           -11.19624490295010
 cs2           1.849473452855880
 a1            62.78808135485872
 a2            29.79890240095949
 cc3           1.532955127356614
 ccs3          114.2231427320000
 a3            90.72808022039182
 nc4           1.452720588257472
 ncc4          109.9374042793200
 var1          161.3149576730383
 hn5           1.017987301180392
 hnc5          118.7560534741794
 dih5          39.76921445961685
 cn6           1.369633060183918
 cnc6          123.4696042639945
 var2         -136.1864695261146
 oc7           1.250258430870259
 ocn7          121.9590048229046
```

```
dih7         -16.87528490843376
hc8           1.115961518258288
hcc8          111.2382844466690
dih8         -79.57850420509111
hcc9          109.8775542182797
dih9          39.41178719547536
hcc10         111.0282442855979
dih10        -74.16382998590493
hcc11         110.3239713187797
dih11         44.17778878481784
cc12          1.499097469730561
ccn12         115.9160562565923
var3         -198.2748394699183
cc13          1.418887337902944
ccc13         118.1524649579006
dih13         156.4517731352625
cc14          1.403722521149343
ccc14         120.0925558358782
dih14         176.9849879012385
cc15          1.418066236483078
cc16          1.421403714285436
cc17          1.414289685888483
ccc17         122.3015836603129
dih17        -26.49473366952892
hc18          1.102479310083090
hcc18         119.8297801262816
dih18        -1.643851268401216
hcc19         122.6951229083375
dih19        -179.1319331963455
hcc20         122.5543560666064
dih20         179.9871864503564
hcc21         118.3143583427292
dih21        -2.481171498151512
nc22          1.400312477925559
ncc22         116.2845939543450
dih22         178.1244170661886
nn23          1.298187316347401
nnc23         112.8496894695807
dih23         181.8774568477920
cn24          1.391816418756323
cnn24         114.3704495695879
dih24         180.0000000000000
cc25          1.424608893156412
ccn25         124.9727819752468
dih25        -1.199759155604062
cc26          1.411147981578717
dih26         182.2842960037103
cc27          1.408935194522842
cc28          1.416701820013942
cc29          1.422177731971850
ccn29         115.8005400527528
dih29         180.2585288969470
hcc30         117.1618829570948
```

```
 dih30       -0.7522371592106530
 hcc31         119.9219180276368
 dih31         180.4052214466115
 hcc32         120.0384044640843
 dih32         178.7353982854251
 hcc33         120.1317279514416
 dih33         180.1738535623223
 hcc34         117.6625110673082
 dih34        -1.592311360815225
%endblock Zmatrix

MD.TypeOfRun  CG
MD.NumCGsteps 1000
MD.VariableCell .false.
SolutionMethod diagon
XC.functional GGA
XC.authors PBE
DM.NumberPulay 7
DM.MixingWeight 0.15
MaxSCFIterations 200
WriteMullikenPop 1
WriteCoorXmol .true.
WriteDM .false.
UseSaveData .true.
SpinPolarized .true.
FixSpin .true.
TotalSpin 0.0
```

Figure A.4: Sample SIESTA input file for an optimization. This particular input file was for optimizing a parallel trans structure in a -1 V/nm electric field.

```
SystemLabel     azo
NumberOfSpecies 6

%block ChemicalSpeciesLabel
 1  6  C
 2  7  N
 3  8  O
 4  1  H
 5 16  S
 6 79  Au
%endblock ChemicalSpeciesLabel

Denchar.TypeOfRun 3D
Denchar.PlotCharge .true.
Denchar.PlotWaveFunctions .true.
Denchar.CoorUnits Ang
Denchar.DensityUnits Ele/Ang**3
Denchar.NumberPointsX 104
Denchar.NumberPointsY 104
Denchar.NumberPointsZ 104
Denchar.MinX -8.0 Ang
Denchar.MaxX 18.0 Ang
Denchar.MinY -8.0 Ang
Denchar.MaxY 18.0 Ang
Denchar.MinZ -20.0 Ang
Denchar.MaxZ 6.0 Ang
~
```

Figure A.5: Sample DENCHAR input file for plotting orbitals and electron density.